Pacific Northwest
NATIONAL LABORATORY

PNNL-33726

New NDA Methods for Thorium Fuel Cycle Safeguards

Mid-project Report

November 2022

B. McDonald
A. Danagoulian
J. Kulisek
J. Rahon
J. Burnett
A. Gilbert
M. Moore
G. Warren
R. Clark
E. Klein
B. Pierson
M. Zalavadia

U.S. DEPARTMENT OF ENERGY

Prepared for the U.S. Department of Energy
under Contract DE-AC05-76RL01830

DISCLAIMER

PACIFIC NORTHWEST NATIONAL LABORATORY
operated by
BATTELLE
for the
UNITED STATES DEPARTMENT OF ENERGY
under Contract DE-AC05-76RL01830

Printed in the United States of America

Available to DOE and DOE contractors from
the Office of Scientific and Technical Information,
P.O. Box 62, Oak Ridge, TN 37831-0062
www.osti.gov
ph: (865) 576-8401
fox: (865) 576-5728
email: reports@osti.gov

Available to the public from the National Technical Information Service
5301 Shawnee Rd., Alexandria, VA 22312
ph: (800) 553-NTIS (6847)
or (703) 605-6000
email: info@ntis.gov
Online ordering: http://www.ntis.gov

PNNL-33726

New NDA Methods for Thorium Fuel Cycle Safeguards

Mid-project Report

November 2022

B. McDonald J. Burnett R. Clark
A. Danagoulian[1] A. Gilbert E. Klein[1]
J. Kulisek M. Moore B. Pierson
J. Rahon[1] G. Warren M. Zalavadia

Prepared for
the U.S. Department of Energy
under Contract DE-AC05-76RL01830

Pacific Northwest National Laboratory
Richland, Washington 99354

[1] Massachusetts Institute of Technology

This page intentionally left blank.

Abstract

This project is developing new nondestructive assay (NDA) safeguards techniques for emergent thorium fuel cycles based on neutron resonance transmission analysis (NRTA), which can assay ^{233}U and ^{235}U when they are present together in a sample with potentially high gamma ray backgrounds from fission products and ^{232}U. Existing passive techniques face large challenges for this task, so new active interrogation methods are needed. This effort is also exploring how gamma ray signatures can complement NRTA for enhanced assayed performance. This project leverages an NRTA system being developed at Pacific Northwest National Laboratory (PNNL) in collaboration with the Massachusetts Institute of Technology (MIT), which uses a commercially available deuterium-tritium neutron generator at short standoff (~2 m). The research team aims to assess the feasibility and performance of these new NDA techniques for the range of relevant samples in thorium fuel cycles. Key advancements described in this mid-project report include NRTA system design for thorium safeguards measurements, characterization of ^{233}U oxide powder at PNNL, a survey of detector technologies suitable for NRTA in high gamma background environments, successful preliminary demonstration of a quantitative isotopic estimation algorithm, and first NRTA measurements of a thorium sample.

This page intentionally left blank.

Summary

Pacific Northwest National Laboratory (PNNL), in collaboration with the Massachusetts Institute of Technology (MIT), is leading this first project to explore using neutron transmission resonance analysis (NRTA) for nondestructive assay (NDA) measurements in future thorium fuel cycle safeguards. This technique exploits unique epithermal resonance structures to quantitatively determine isotopic contents in a sample. Until recently, NRTA has been limited to large-scale accelerator facilities. Now it is possible to use NRTA with portable neutron sources and relatively short (2 m) flight paths (Figure S 1). NRTA is particularly well-suited for assaying ^{233}U, ^{235}U, ^{232}Th, and possibly other isotopes of safeguards interest when they are present together in a sample. Many existing techniques are challenged to accurately assay such multi-isotope mixtures.

The research team examined two notional measurement scenarios to assess NRTA for thorium fuel cycles. These serve as high-level examples that could be broadly encountered in future safeguards inspections. The starting scenario for quantitative NRTA measurements was with gram-level quantities sampled from process lines or storage containers. Another potential scenario is online monitoring of process lines in a molten salt reactor (MSR). Both scenarios are challenging because of likely very high gamma fields from ^{232}U and its progeny, ^{233}U, and fission/activation products. One aspect of making NRTA practical for these scenarios is incorporating a neutron detector that can operate in high gamma radiation fields without misclassifying neutron events. Furthermore, the large gamma ray signals also present additional information that can be used to constrain NRTA analysis. Both these aspects were investigated.

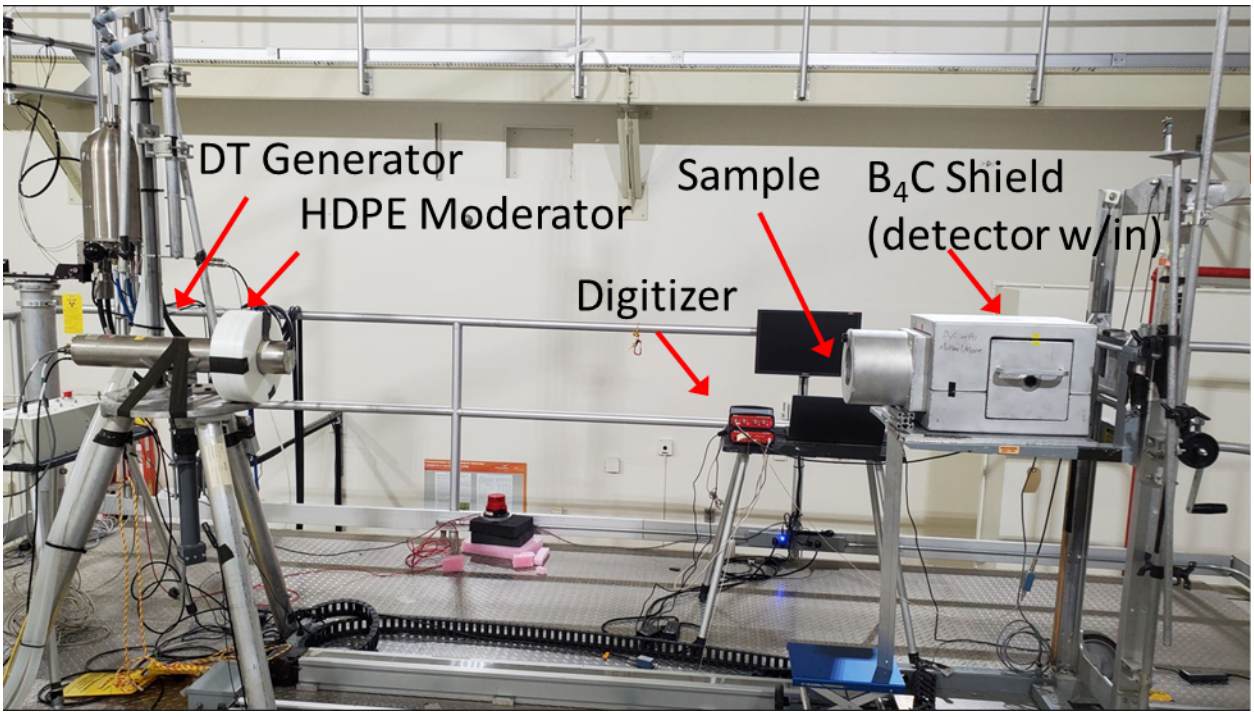

Figure S 1. Photograph of the neutron transmission resonance analysis experimental setup at PNNL.

In the first year of this project, the research team completed a diverse range of tasks to demonstrate the feasibility of NRTA for thorium fuel cycle NDA. The research team

characterized ^{233}U material at PNNL, identified additional relevant sources for testing, designed and fabricated custom NRTA source holders, explored sample measurement configurations in modeling space, surveyed and down-selected viable neutron detectors, made initial NRTA measurements with a thorium source, and developed an algorithm that initially works very well on measured data.

Key findings included:

- The ^{233}U material at PNNL was determined to be very pure (99.996%) with gamma/charged-particle coincidence analysis. This material will be helpful for testing quantitative NRTA methods. Samples with ^{232}Th, ^{235}U, ^{233}U, ^{238}U, and ^{239}Pu are available for measurements and can be stacked to create different isotope areal densities for testing quantitative algorithms.
- Initial analysis on NRTA data of ^{232}Th showed that it was possible to detect resonances of that isotope in a relevant sample configuration (Figure S 2).
- An initial analysis algorithm performed remarkably well for accurately estimating uranium isotopics from NRTA data of measured depleted uranium (DU) and highly enriched uranium (HEU) objects (Figure S 3).

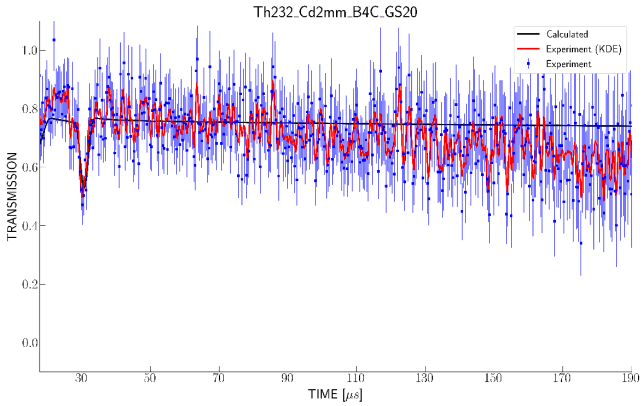

Figure S 2. Neutron transmission versus time for a ^{232}Th source. The calculated line (from evaluated nuclear data file data and system timing resolution) is black. The experimental data is plotted in blue, and the red line is the smoothed data with a Gaussian kernel density estimate (KDE). Bin width is 333 ns.

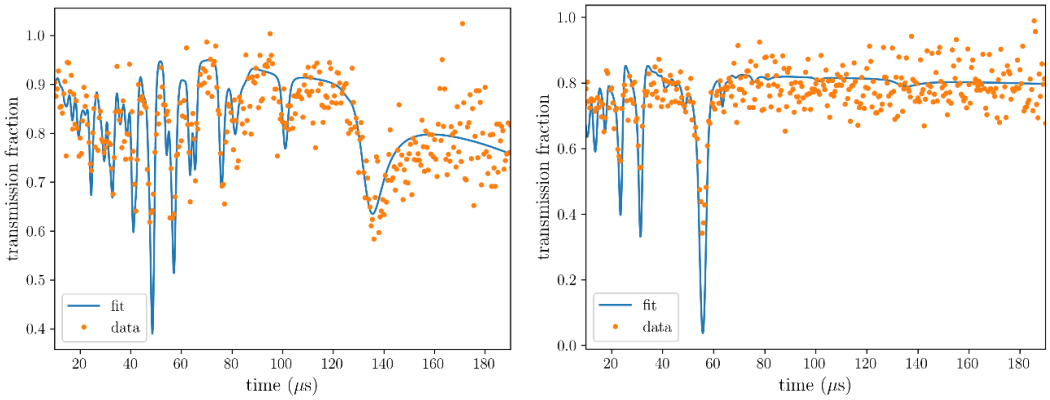

Figure S 3. The figure on the left shows fit of an NRTA measurement to measured data of an HEU plate. The figure on the right shows fit of the NRTA time of flight spectrum (blue) and the measured data (orange) for NRTA data of a depleted uranium plate.

This page intentionally left blank.

Acknowledgments

This research was supported by the National Nuclear Security Administration Office of Defense Nuclear Nonproliferation Research & Development. Ethan Klein was funded by an appointment to the Nuclear Nonproliferation International Safeguards Fellowship Program sponsored by the National Nuclear Security Administration's Office of International Nuclear Safeguards (NA-241).

This page intentionally left blank.

Acronyms and Abbreviations

CCD	charge-coupled device
CMOS	complementary metal oxide semiconductor (camera)
CZT	cadmium zinc telluride
DNN R&D	NNSA Office of Defense Nuclear Nonproliferation Research and Development
DT	deuterium tritium
DU	depleted uranium
ENDF	evaluated nuclear data file
HALEU	high assay low enriched uranium
HDPE	high-density polyethylene
HEU	highly enriched uranium
HPGe	high-purity germanium
IVAC	Isotope Verification for Arms Control (project)
KDE	kernel density estimate
LEU	low enriched uranium
LFTR	lithium fluoride thorium reactor
MCP	microchannel plate
miniHDND	mini high-dose neutron detector
MIT	Massachusetts Institute of Technology
MSR	molten salt reactor
MSRE	Molten Salt Reactor Experiment
NDA	nondestructive assay
NNSA	National Nuclear Security Administration
LANL	Los Alamos National Laboratory
LSF	Low Scatter Facility
MCNP	Monte Carlo N-Particle
NRCA	neutron resonance capture analysis
NRTA	neutron resonance transmission analysis
PMT	photomultiplier tube
PNNL	Pacific Northwest National Laboratory
PSD	pulse-shape-discrimination
RPL	Radioactive Processing Laboratory
TOF	time of flight

This page intentionally left blank.

Contents

Figures

Tables

This page intentionally left blank.

1.0 Introduction

Current safeguards nondestructive assay (NDA) techniques face significant challenges and uncertainty as to whether they will effectively translate to thorium fuel cycle measurements (Worrall et al. 2016; Dion et al. 2021; Swift et al. 2020; Kovacic et al. 2018). A diverse range of thorium-based reactor designs would include heterogenous nuclear material with multiple fissile and/or fertile isotopes. One challenge is accurately measuring ^{233}U and ^{235}U content in a sample material when they are present together (and in possibly very high gamma backgrounds from fission and activation products) and ^{232}U progeny (Evans et al. 2021). Established and some emerging techniques are likely inadequate for many scenarios because of the typical high gamma background, low spontaneous fission factor, and limited gamma ray signatures of ^{233}U. Limitations in passive signatures point to a need for new active interrogation methods. Another NDA challenge is quantitative assay of ^{232}Th mass (Evans et al. 2021).

Pacific Northwest National Laboratory (PNNL), in collaboration with the Massachusetts Institute of Technology (MIT), is developing neutron resonance transmission analysis (NRTA) as a promising solution to these emerging safeguards challenges. NRTA provides isotopic data about a sample via time-of-flight (TOF) neutron measurements that exploit unique epithermal neutron resonance cross-sections. NRTA has been recently demonstrated to work with commercially available deuterium-tritium (DT) neutron generators in short standoff (~2 m) geometries in reasonable measurement times (i.e., less than two hours)(Klein, Naqvi, Bickus, et al. 2021). If successful, this will enable a new NDA approach in thorium fuel cycles.

The specific objectives of this effort include:

- Demonstrating the feasibility of NRTA for ^{233}U and ^{235}U assay by performing modeling and laboratory experiments with relevant samples. This includes incorporating a neutron detector that can discriminate neutrons from gamma rays in high gamma fields and developing quantitative algorithms to analyze NRTA data.
- Showing how gamma ray signatures can complement NRTA for enhanced assay performance. The research team hypothesizes that gamma ray data will help constrain materials in a sample and improve isotope mass quantification with NRTA. This includes passive singles and coincidence spectra and neutron capture resonance analysis (NRCA).
- Raising the technology readiness level (TRL) of portable NRTA by performing measurements on representative samples in a laboratory setting and show how NRTA could be practical for safeguards.

These objectives align with recommended research efforts described in a 2021 report for the National Nuclear Security Administration (NNSA) Office of Defense Nuclear Nonproliferation Research and Development (DNN R&D) (Evans et al. 2021) (italicized texts are PNNL comments):

1) Verify feasibility of basic methods and generic technologies

    a. Active interrogation with progressively modulated neutron spectrum to interrogate different energy regions of the neutron-induced fission cross section. *The NRTA method essentially does this by creating a broad range of energies that interrogate the sample and are measured by their time of flight.*

2) Quantify sensitivity limits

a. NDA (both gamma and neutron) of pure as well as composite items and in the presence of accidental or deliberate interferences. *Sensitivity limits for NRTA in various sample types with and without gamma ray data will be explored.*

3) Technological upgrade and/or modification

a. Neutron detector resiliency in high-gamma background environment (due to the presence of ^{232}U). *The research team is assessing impacts of high gamma ray backgrounds for various neutron detectors and taking steps to mitigate backgrounds for NRTA.*

b. Active interrogation-based systems using neutron generators. *This is a core aspect of portable NRTA.*

This report summarizes progress at the approximate midpoint of the project life cycle. After a brief background on related NRTA work, Section 2.3 describes the system design for a safeguards NRTA system, including a study of relevant samples with modeling results. Section 4.0 describes detector requirements and considerations for thorium fuel cycle NRTA and gamma ray measurements. Section 5.0 summarizes preliminary measurements and analysis, including characterizing of ^{233}U material at PNNL. Section 6.0 describes the development of a quantitative isotopic content algorithm. Section 7.0 provides key findings for the first year and plans for the second year.

2.0 Background

The NRTA technique provides isotopic information about a sample by analyzing the magnitude and energy of absorption lines in TOF neutron spectra (e.g., 1-50 eV range). In this energy range there are unique resonances that can identify and quantify isotopes of interest. NRTA can be used to estimate the linear density of isotopes present in a sample (Hasemi et al. 2015). NRTA has been considered for characterization of fresh ((Klein, Naqvi, and Danagoulian 2021; Adrian S Losko et al. 2016)) and spent fuel (Chichester et al. 2012), assay of fissile content in Fukushima corium (Tsuchiya et al. 2019), and for arms control verification (Engel et al. 2019). NRTA has been used to assay the ^{235}U and ^{238}U content in fresh fuel pellets with a pulsed Linac neutron source (Behrens et al. 1984). NRTA is also sensitive to many fission products, which if assayed, can provide data about the irradiation history of the material provided the fission products are in sufficient quantity (Sterbentz et al. 2011). With a time-resolved imaging detector and tomographic reconstruction techniques, recent work has shown it is possible to derive 3D isotopic densities of a U-20Pu-10Zr-3Np-2Am (weight percent) fuel slug (Adrian Simon Losko et al. 2022). Most prior work in NRTA required the use of large neutron sources in accelerator facilities, which is not practical for safeguards measurements.

MIT recently demonstrated that NRTA can be achieved with commercially available DT neutron generators in short standoff (~2 m) geometries in reasonable measurement times (i.e., less than two hours) (Klein, Naqvi, Bickus, et al. 2021). This demonstration opened the door to new applications where portable systems can be set up in typical laboratory spaces compared with 20 m standoffs at accelerator facilities. The MIT team, led by Professor Danagoulian, has developed NRTA as part of the Consortium of Verification Technologies (CVT) and the Consortium for Monitoring, Technology, and Verification (MTV) (Engel et al. 2020; Klein, Naqvi, and Danagoulian 2021). In the last two years, MIT has collaborated with PNNL on developing NRTA for arms control verification through the Isotope Verification for Arms Control (IVAC) project (FY21-PL-PD2Nc-P18). NRTA also shows much promise for practical safeguards measurements.

Figure 1 shows the distinct resonance structure for total neutron cross-section isotopes of interest including ^{233}U and ^{235}U, which provide strong discriminatory features. Other isotopes of interest, ^{238}U and ^{233}Pa (decays to ^{233}U) also have distinguishing resonances. The fertile material, ^{232}Th, only has two resonances (21.8 and 23.4 eV) in the range plotted. ^{233}U has strong resonance structures from 1.5-3.0 eV and at 10.4 eV, among others. ^{234}U, which has a strong resonance at 5.2 eV, may also be present in high fractions (e.g., ~25% of uranium in fuel salt at equilibrium in a liquid fluoride thorium reactor (LFTR) (Reed et al. 2022). The cross sections for ^{232}U were not included, because the expected concentrations are so low as to not have an impact on neutron attenuation. Those low concentrations (up to hundreds of ppm) can create large radiation fields that can potentially overwhelm many gamma ray and neutron detectors. Quantitative assay performance is limited by a combination of background terms and the macroscopic cross-section for a given isotope in the sample. For items such as fuel pellets or salt samples, this translates to thicknesses on the order of centimeters or less.

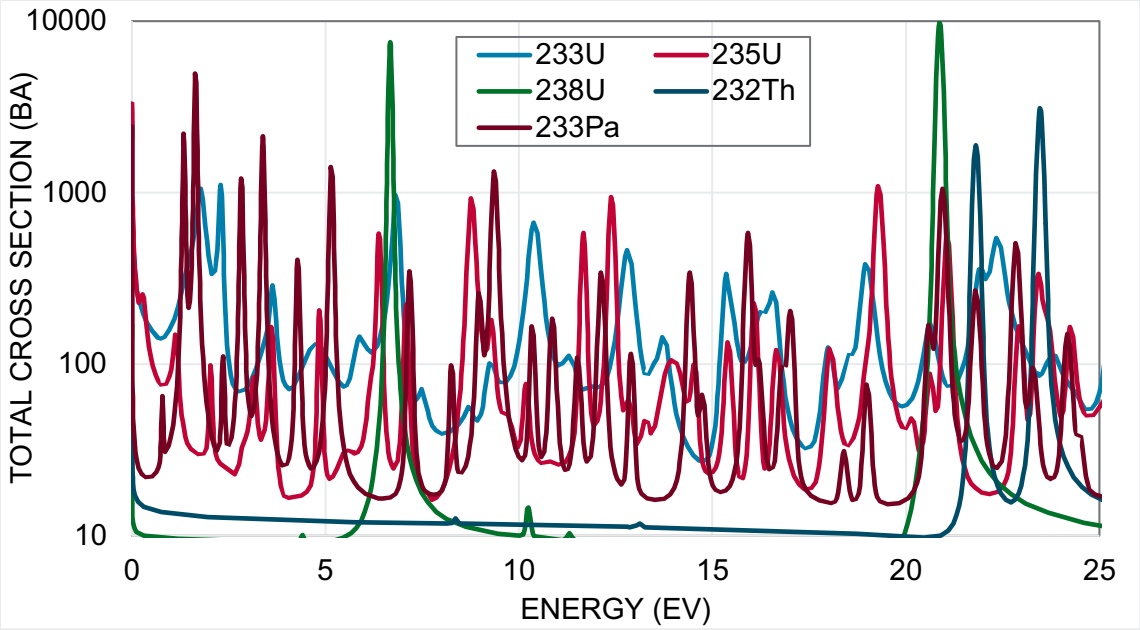

Figure 1. Total neutron cross-section data for some isotopes of interest (evaluated nuclear data file (ENDF))/B-VII.1.1.

A 2021 report that evaluated the feasibility of existing NDA techniques for thorium fuel cycle safeguards noted that quantitative assay of ^{232}Th with neutrons was difficult or impractical (Evans et al. 2021). Assay of ^{233}U was possible in principle with some existing techniques, but it was not clear if these would be able to assay ^{233}U and ^{235}U together. Table 1 is modified from Evans et al. (2021) and includes an additional column that describes the feasibility of NRTA for each assay target. The column on passive assay was removed (all “not feasible”). Because of the unique resonances among the isotopes of interest, NRTA is very likely feasible for nearly all the material types and assay targets considered in the table. Moreover, it is also sensitive to isotopes not included in the table that are of safeguards interest (e.g., ^{233}Pa and ^{239}Pu). The only material type that may not be feasible is ThC because of the low-Z component, which will reduce resolution in the TOF spectrum due to scattering and moderation. However, the research team has shown that it is possible to observe resonances in a highly enriched uranium target that was surrounded by an acrylic container, so depending on the sample configuration, it may still be possible to quantitatively assay ^{232}Th in a ThC sample.

Table 1. Summary of the preliminary evaluation of the feasibility of neutron NDA techniques with NRTA included (adapted from (Evans et al. 2021)).

Assay Target	Material Type	Active Assay	Self-interrog.	NRTA Note
^{232}Th	^{232}Th metal	Difficult, fast neutrons only	Not feasible	Feasible
	$^{232}ThO_2$	Difficult, fast neutrons only	Not feasible	Feasible
	(^{233}U, Th)O_2	Not feasible	Not feasible	Feasible
	(Enriched U, Th)O_2[(a)]	Not feasible	Not feasible	Feasible
	ThC[(a)]	Difficult, fast neutrons only	Not feasible	Likely feasible
	Th(FLiBe) salt[(a)]	Difficult, fast neutrons only	Not feasible	Feasible
^{233}U	^{233}U metal	Feasible, similar to ^{235}U	Not feasible	Feasible
	$^{233}UO_2$	Feasible, similar to ^{235}U	Difficult, potentially feasible	Feasible
	$^{233}UF_4$	Feasible, similar to ^{235}U	Likely feasible	Feasible

(a)Material type not included in the simulations or measurements (in Evans et al. 2021).

2.1 Safeguards Scenarios

NRTA has not been evaluated or developed for thorium fuel cycle safeguards, and it is likely useful for a range of potential NDA scenarios for bulk nuclear material. The research team examined two notional measurement scenarios to assess NRTA for thorium fuel cycles. These serve as high-level examples that could be broadly encountered in future safeguards inspections. Specific reactor or facility safeguards was not part of this effort, but some examples in the literature were used to select relevant sample compositions and dose rates. These scenarios were explored with radiation transport modeling to understand the range of relevant sample parameters (e.g., chemical form) and help design samples for proof-of-concept experiments.

The starting scenario for quantitative NRTA measurements of ^{233}U and ^{235}U is with gram-level quantities sampled from process lines or storage containers and put into holders. This scenario would be akin to what is currently done in physical inventory verification (PIV) safeguards inspections at nuclear facilities with systems like the Combined Procedure for Uranium Concentration and Enrichment Assay (COMPUCEA (Berlizov et al. 2016)). In this application, the samples would be in fixed geometries and isotopes within the sample and could be constrained based on knowledge of the facility and the container from which it was sampled.

In recent modeling studies for a LFTR, dose rates from 100 mL samples of irradiated fuel and blanket salt were estimated to have gamma dose rates of 530 and 46.5 rem/hr, respectively, at 1 ft for material that has cooled 3.65 days. For neutrons, the dose rates were 0.0029 and 0 rem/hr (Reed et al. 2022). The sample size of 100 mL (203 and 443 grams of fuel and blanket salt, respectively) is much larger than needed for NRTA, so dose rates could be lower by approximately two orders of magnitude. Nevertheless, the upper dose rates will be considered for detector requirements. Another report considered a similar 700 rem/hr gamma dose rate as

a threshold for which neutron detectors should be able to function in molten salt reactor NDA measurements (Sagadevan et al. 2021).

Another potential scenario is online monitoring of process lines in a molten salt reactor (MSR). This is a more challenging application because of the extremely high gamma ray fields, greater sample thicknesses, potentially large neutron backgrounds, and potentially dynamic isotope concentrations. In the early 1970s at the Molten Salt Reactor Experiment (MSRE), a small hole was made in the concrete biological shield to perform gamma spectroscopy measurements on a heat exchanger of the MSRE. The gamma ray dose rate through the hole was more than 1000 R/h, requiring the gamma spectrometer to be further collimated and shielded to acquire useful data (Houtzeel et al. 1972). NRTA measurements would likely also need to be in locations where the gamma ray and neutron backgrounds can be reduced with specialized shielding and collimation or by nature of the process being monitored. For example, it may be more practical to measure lines that do not include fission products like the blanket salt processing or decay tank in a LFTR design (Figure 2). Initial modeling of this scenario was conducted and described in Section 3.2.

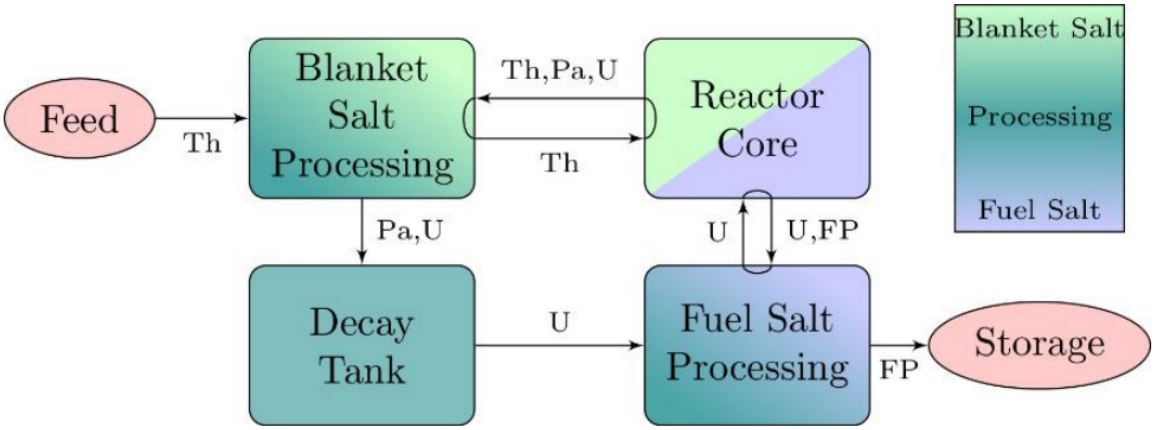

Figure 2. High-level fuel cycle flow chart of the LFTR design, from (Reed et al. 2022).

2.2 Leveraging Gamma Ray Signatures

Gamma ray NDA measurements can provide an independent measure of sample isotopics. The research team hypothesizes that these data can be used to constrain the most abundant isotopes in the sample and improve uranium assay accuracy and precision (Figure 3). Gamma-ray data could be particularly useful for isotopes that have some overlapping resonances. Moreover, typical inverse problem approaches that minimize the difference between measured and expected data perform better when there are fewer fitting variables (number of target assay isotopes, in this case). Such an algorithm was used in this project and is described in Section 6.0. The research team is exploring three types of gamma ray measurements for this purpose: 1) passive singles spectroscopy with cadmium zinc telluride (CZT) and high-purity germanium (HPGe) detectors, 2) passive coincidence spectroscopy with HPGe detectors (possibly also CZT), and 3) neutron capture gamma rays produced during NRTA measurements. These measurement approaches are discussed below.

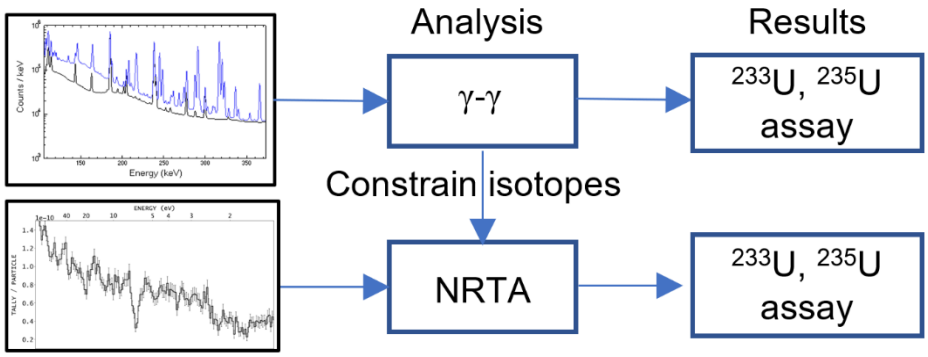

Figure 3. High-level analysis framework envisioned for NRTA and gamma ray assay.

Gamma ray singles measurements could be made on the same sample configurations used in NRTA in a sequential fashion. Some shielding or collimation may be needed to reduce the effective sample size to limit detector counting rates. Passive singles spectroscopy may not be able to assay ^{233}U in some samples because the low-energy gamma rays from ^{233}U can be obscured from fission product and ^{232}U backgrounds. Incorporating singles measurements would also be straightforward in a safeguards context, as these types of detectors are in current use.

Passive coincidence spectroscopy has recently been shown to assay ^{233}U in high-fission-product backgrounds in surrogate molten salt reactor (MSR) samples (Burnett 2022). Sample masses for coincidence spectroscopy must be much smaller than those used for NRTA (milligram versus gram levels) to not overwhelm the detectors. Coincidence data could also be useful for constraining the types and amounts of isotopes for NRTA analysis, but with a higher operational overhead and a typically non-mobile system of multiple HPGe detectors. One potentially promising area of future development is using two CZT detectors in a coincidence configuration. These do not require cooling, have higher count rate capability than HPGe, and may have sufficient energy resolution to assay ^{233}U in mixed backgrounds.

In the course of NRTA measurements, neutron capture gamma rays are also produced in the sample and these can identify the sample matrix materials and impurities (Tsuchiya et al. 2019). NRCA is a close relative of NRTA and has been used for years to perform quantitative elemental and isotopic analysis on samples (Postma et al. 2017). Gamma rays produced at certain times after the neutron pulse (corresponding to a specific neutron energy) are specific for each nuclide. To make use of this signal, a gamma ray detector is placed near the sample during NRTA measurements. To reduce gamma backgrounds, a fast neutron detector can be used, in addition to the gamma sensor, so only events that include a fission neutron and a capture gamma ray are recorded. MIT is evaluating whether this is feasible for samples with large gamma emission rates.

2.3 Experimental Setup

This project leverages and builds upon an NRTA capability developed at PNNL in an arms control project (Isotope Verification for Arms Control (IVAC, FY21-PL-PD2Nc-P18). A photograph of the setup at the PNNL 318 Building, Low Scatter Facility is shown in Figure 4. A Thermo ScientificTM P 385 DT neutron generator (at left in photo) creates 14.1 MeV neutrons that are moderated in a custom lead and high-density polyethylene (HDPE) collars (Figure 5). The design of the moderator was a significant effort that enhanced epithermal neutron

production, limited gamma background, and achieved sufficient energy resolution (via compact moderation path) (Zalavadia et al. 2021). Close-up photos of the DT generator and moderator are shown in Figure 5. The IVAC project determined settings for the pulse structure of the generator to limit “wrap-around” neutrons and maintain high flux rates. The generator pulse frequency was 5000 Hz with a duty factor of 3.5%, so the pulse widths were 7 μS. Typically, the DT generator was run at 130 kV and 35 μA for measurements less than two hours. Moderated neutrons drift across a 2.0 m distance and pass through a sample placed in front of a collimated detector shield assembly (at right in photo). Between the sample and the detector is a 2 mm thick cadmium sheet to stop thermal neutrons. Neutrons are attenuated depending on the sample isotope’s macroscopic cross-section and then detected by a 5 mm thick GS20 (Scintacor, Inc) ^{6}Li glass scintillator coupled to a ø7.6 cm photomultiplier tube (PMT). The detector is inside a B_4C shield that reduces off-axis neutrons (e.g., room return) and is readout by a CAEN digitizer (DT5730SB). The shield has a puzzle box design to remove direct streaming paths for neutrons. The timing signal from the DT generator pulse is fed into the digitizer, which computes the difference between the neutron pulse and the detector signals as the TOF for each event in 250 ns bins. A CAEN high voltage supply applies bias to the PMT.

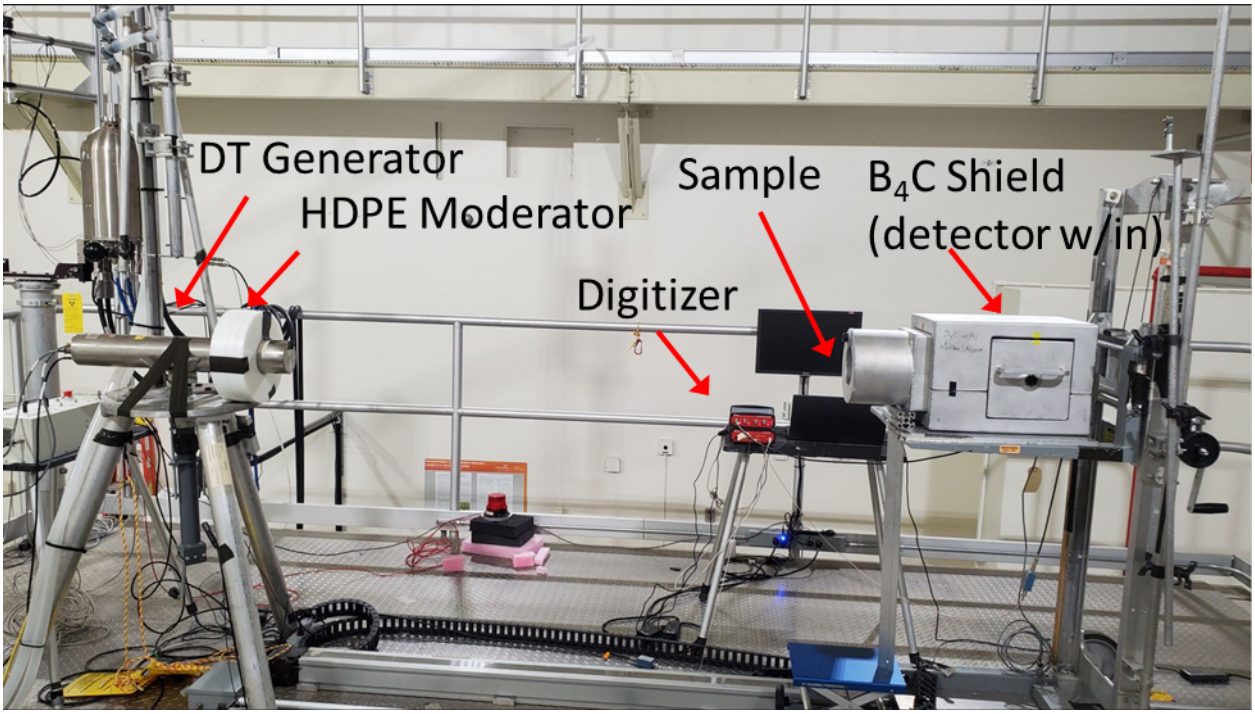

Figure 4. Photograph of the NRTA setup with 2.0 m standoff.

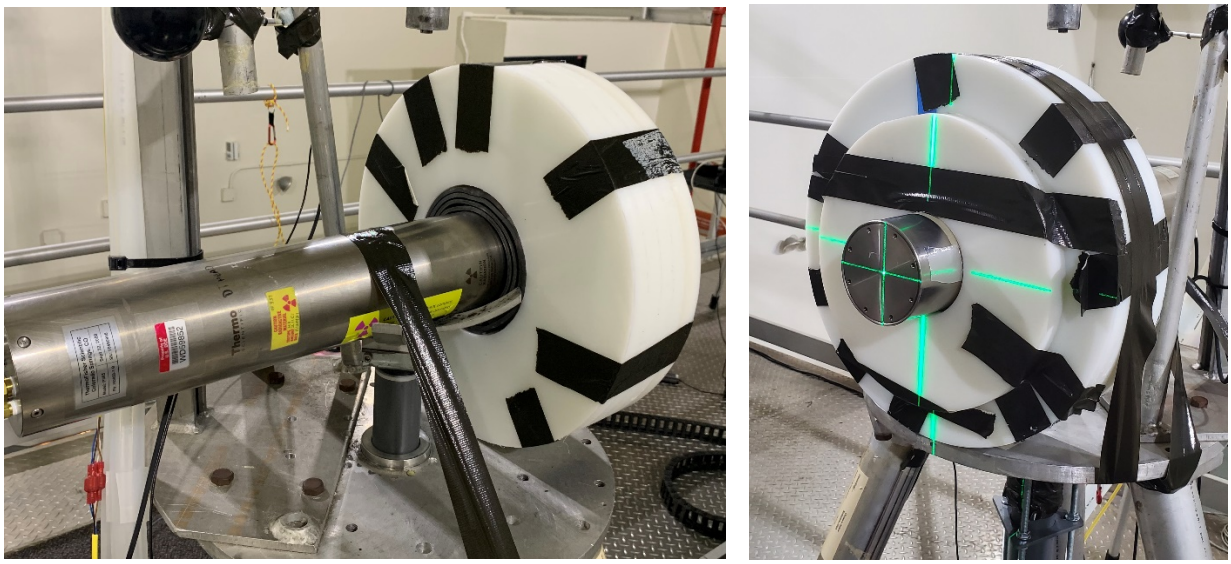

Figure 5. Photographs of the DT generator with custom lead/HDPE sleeves from rear (left) and front (right) views. The green lines are from a laser level used in source/detector alignment.

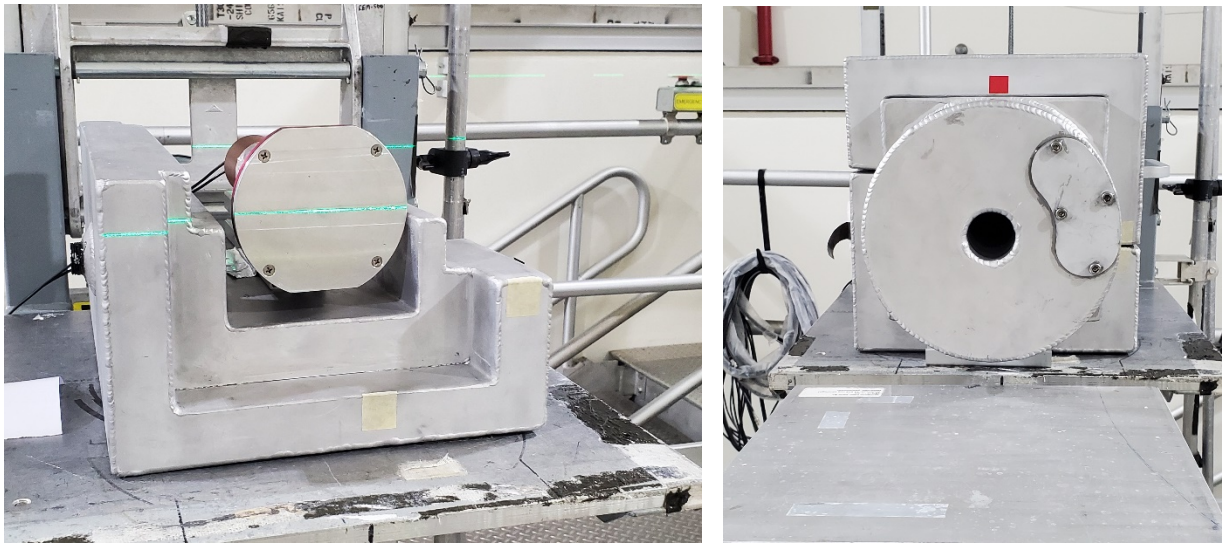

Figure 6. Photographs of the GS20 detector within the partially assembled B_4C shield (left), and the assembled shield with ø42 mm collimator attached (right).

This page intentionally left blank.

3.0 System Design

With a functional NRTA setup from the IVAC project as a starting point, the research team considered how the current system could be adapted and enhanced for the defined thorium fuel cycle measurement scenarios. This includes survey and selection of relevant samples forms, a preliminary sensitivity analysis, design of a sample holder suitable for gamma and neutron measurements, and design refinements of the shielding collimators. Key differences from IVAC measurements include 1) potentially very radioactive samples, and 2) a higher emphasis on data analysis, algorithm development, and uncertainty quantification. The latter is needed for isotope abundance measurements as opposed to mere detection.

3.1 Sample Development

Suitable material forms for NRTA include powders, salts, fluorides, metals, ceramics, etc. Small items (e.g., lead pigs, fuel pellets) containing such samples can be accessible with NRTA. Lead moderately attenuates epithermal neutrons and has no resonances in the energy range of interest. Tungsten on the other hand, has large resonances. Hydrogenous samples are generally not well-suited because of the large scattering and absorption cross-sections for the neutron energies of interest.

The research team started by looking for relevant samples available at PNNL for testing NRTA. A key find was a 19 g ^{233}U oxide powder sample. According to the PNNL Radioactive Material Database, this material was very pure ^{233}U and was assayed via gamma energy analysis in 2011. According to that assay, 92% of the activity of the sample is from ^{233}U, with the rest from ^{232}U and its progeny and ^{241}Am. The specific activity of the material is ~10 mCi/g. Gamma ray singles and coincidence spectra were collected on aliquots of the ^{233}U material available at PNNL and the results are described in Section 5.1. To yield detectable signal-to-background ratios for the ^{233}U resonances, the sample thicknesses were informed using the iNeutron Imaging Toolbox (iNEUIT) which estimates transmission percentages (Zhang et al. 2019). Each sample thickness was selected as 1.2 mm to provide sufficient resonance contrast (~25% attenuation) at an approximate ~1.5 g/cm^3 tap density. With only 19 g available, the research team planned to make three to four 4 g stackable ^{233}U samples to measure the effects of increasing areal density of ^{233}U in the neutron beam and test quantitative isotope concentration algorithms. A ø50.8 mm sample diameter was chosen to achieve samples around 4 g. Larger-diameter samples (and collimators) would enable higher detector counting rates and lower measurement times, but the research team was limited by the available material.

The research team identified other samples of interest available at PNNL for testing. These included:

- A steel-encapsulated 3 mm thick ^{232}Th metal source (Isotope Products, Isotrak)
- Thorium oxide (thoria) powder
- Low enriched uranium (LEU) powder samples (up to 5 wt.%)
- Highly enriched uranium (HEU) metal plate
- DU metal plate
- High-assay low-enriched uranium (HALEU) metal mini-plates (90% U, 10% Mo, 1 in. x 4 in.)
- Various unirradiated salts used in MSRs with depleted uranium

- Non-radioactive materials such as tungsten and indium useful for testing (e.g., determining backgrounds).

These samples and the ^{233}U can be stacked in different configurations to create different effective masses of nuclear materials in the measurement beam region, which will be very helpful for algorithm development and testing.

3.2 Radiation Transport Modeling

The research team presented a paper at the Annual Institute of Nuclear Material Management Conference that described the modeling results (McDonald et al. 2022), which are described in this section, along with new results.

Radiation transport modeling was used to help design these system components and to generate simulated TOF spectra of samples containing various relative concentrations of ^{233}U and ^{235}U. This was a preliminary step to develop the capability to extract ^{233}U and ^{235}U concentrations from data taken from actual measurements when such data become available and to help determine suitable sample sizes. Differences in the simulated TOF spectra within specific time regions can be used by algorithms to quantify the levels of ^{233}U and ^{235}U in fixed-geometry samples.

MCNP6.2® (MCNP), a Monte Carlo code with three-dimensional geometry, was used to conduct all of the radiation transport simulations (Werner et al. 2018). A detailed model of the Low Scatter Facility at PNNL was included as the environment for the TOF measurements within the overall MCNP model. A polyethylene (poly) -moderated DT neutron generator was included in the model. The source-to-detector standoff distance was 200 cm. This MCNP model is depicted in Figure 7, generated using Visual Editor 6.1 (Schwarz et al. 2018). The Low Scatter Facility at PNNL is a room that is 16.5 m and 10 m parallel and perpendicular, respectively, to the neutron flight direction, and is 9 m high from floor to ceiling. It has 30 cm-thick concrete walls.

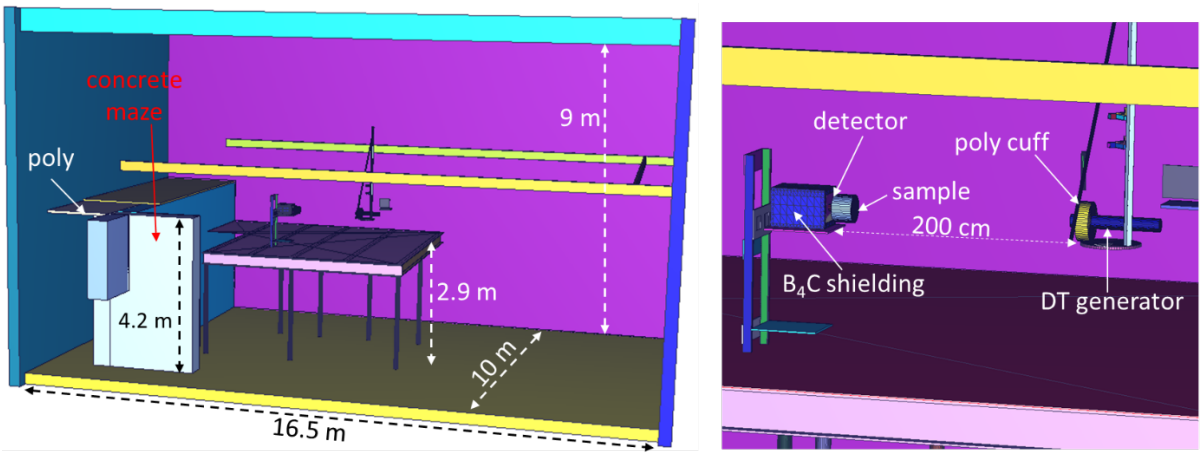

Figure 7. View of the model geometry (left) and zoomed-in view of the NRTA setup (right).

The MCNP model of the DT neutron generator was of the Thermo Scientific™ P 385. A non-ideal (i.e., non-symmetric) pulse width of 10 μs was considered in the model. However, the pulse period of 200 μs was not considered, and therefore neutron background contamination in the signal prior to 200 μs from late-arriving scattered neutrons from previous neutron pulses

("wrap-around") was neglected. To moderate the 14 MeV neutrons, an annular poly cuff, 10 cm thick and wide along the radial and axial directions, respectively, was placed around the DT neutron generator, centered at the axial location of the DT target plane. The neutron yield of this DT generator is 3×10^8 n/s.

The modeled neutron detector was a cylindrical GS20 ^{6}Li glass scintillator (Scintacor) having a diameter of 51.8 mm and thickness of 5.5 mm. The PMT is included in the model, and the detector is collimated and shielded by B_4C and cadmium to reduce background from thermal neutrons. The neutron counts were calculated by tallying the ^{6}Li(n, t)^{4}He reaction rate within the GS20 crystal, and therefore gamma ray interactions were not considered. The neutron capture peak is around 1.6 MeV electron-equivalent (ee) in this material, so high-energy gamma rays can be misidentified as neutrons, and various techniques can be used to enhance particle discrimination (Wang et al. 2016).

The sample area, thickness, and density must be within certain ranges to enable partial transmission of neutrons at the resonances of interest and reasonable measurement times. The areal densities of target isotopes must not be so large to completely attenuate the incident neutrons, otherwise changes in the intensity of the resonances may be harder to discern (e.g., instead of looking at changes in trough intensity, one must measure the change in trough width). The research team modeled the PNNL ^{233}U material with 2 mm thickness and 57 mm diameter. Figure 8 shows some MCNP results with the nominal sample geometry described above and the PNNL material for ^{233}U oxide. Clear resonance dips are seen in the TOF spectra near 1.5 eV for ^{233}U and 11 eV for ^{235}U.

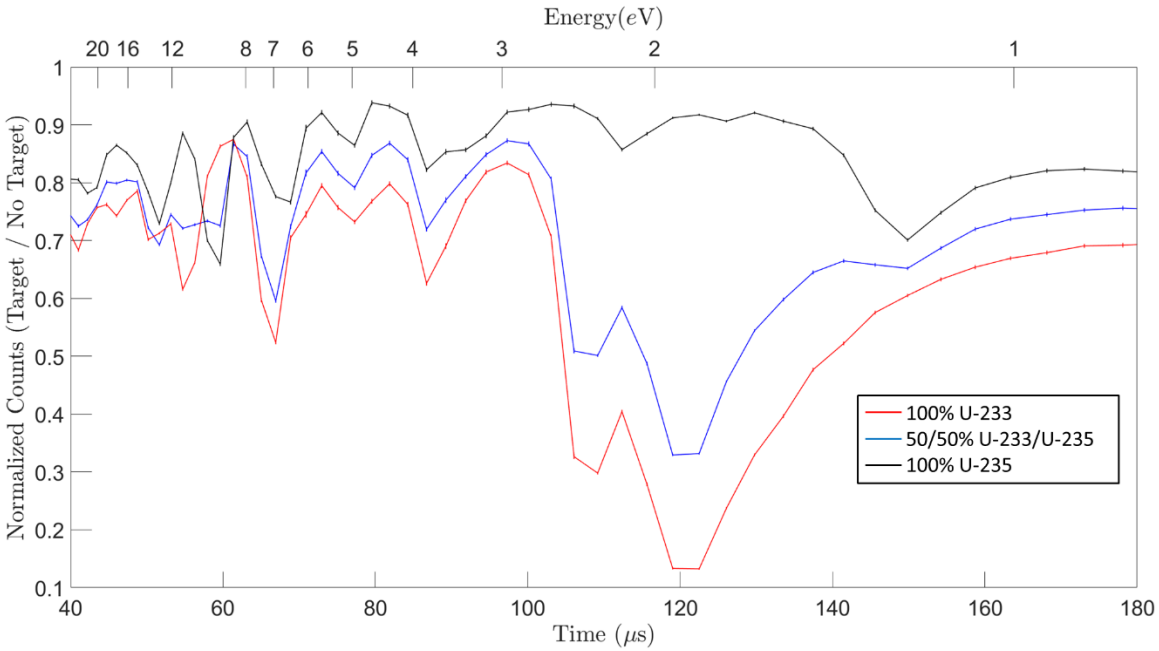

Figure 8. MCNP-generated NRTA results with logarithmically spaced time bins. Note that the open beam (no target) data are used to remove some background terms. The black line is 100% ^{235}U, the blue line is an even mix of the two isotopes, and the bottom (red) line is for 100% ^{233}U. One standard deviation error bars are plotted for each data point, based on statistical uncertainty in the simulations.

For the process monitoring application, epithermal neutrons would need to transmit through a material such as Hastalloy-N, used in the MSRE for its corrosion resistance. The research team created a simulation with the same PNNL material as before and surrounded it with a 3/8 in. Schedule 10 pipe (~1.7 mm wall thickness). Figure 9 shows the results for this scenario, one with an aluminum container with 0.5 mm wall thickness, and one with no encapsulation (i.e., bare), for comparison. The Hastalloy attenuates the neutrons more than the aluminum, but resonance structures are still discernable. Thus, such materials are likely suitable for quantitative NRTA measurements. This is the first indication that the approach may be applicable to MSR safeguards for monitoring nuclear material concentrations.

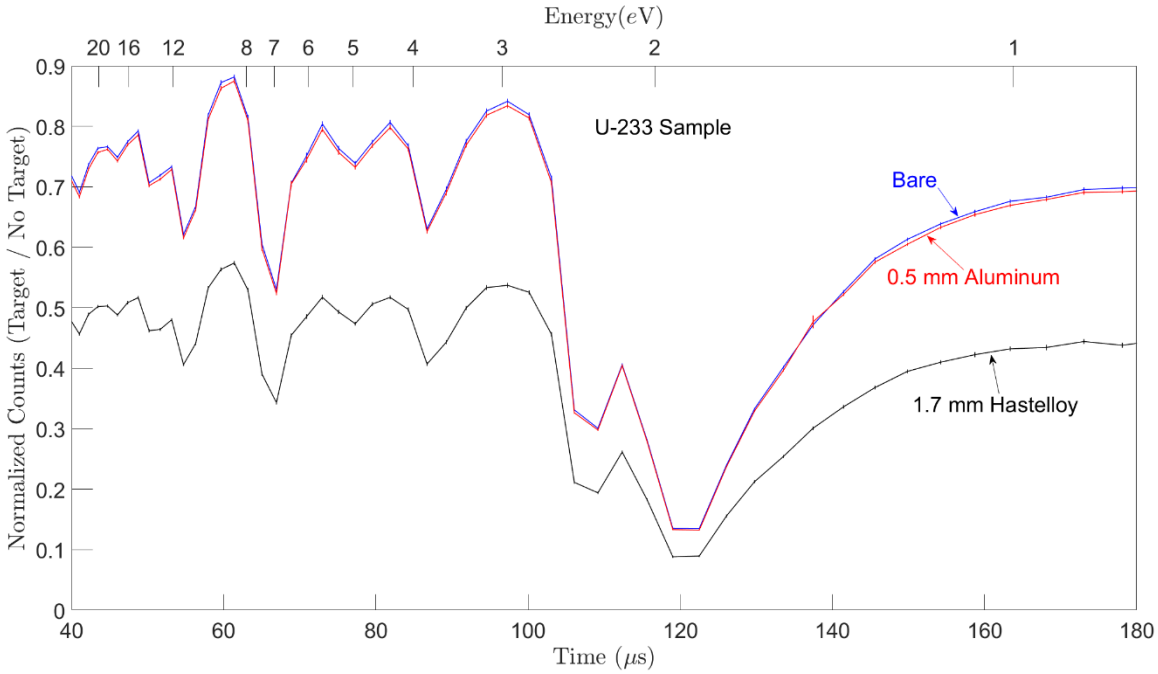

Figure 9. Normalized neutron count rate versus time and energy in the GS20 neutron detector in response with a $^{233}UO_2$ sample and aluminum and Hastalloy-N containers.

The research team also performed simulations of different sample forms, including initial fuel salts for MSRs. One composition of fresh fuel was taken from (Betzler et al. 2017), where the highest mass fraction was ^{232}Th . A nominal 1 mm sample was considered. In Figure 10, the detected resonances from ^{232}Th and ^{238}U are discernable, and the largest trough (at ~22 eV) from ^{232}Th show only a 10% attenuation, indicating that thicker samples could be used. Importantly, the low atomic number constituents of the salt do not greatly attenuate the epithermal neutrons.

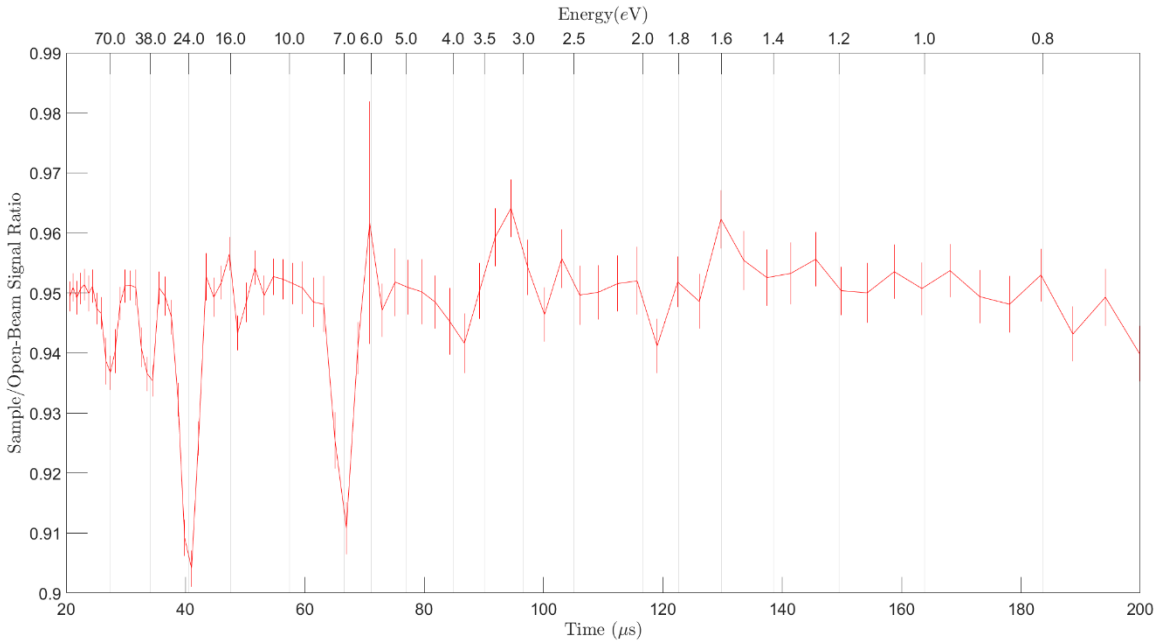

Figure 10. Normalized neutron count rate versus time and energy in a GS20 neutron detector for a 1 mm thick nominal MSR initial fuel salt, divided bin-by-bin by the open beam response (no sample).

3.3 Sample Holder Design and Fabrication

The ^{233}U material is a powder and required containment for the NRTA measurements. A holder was developed to securely contain the powder, to minimally attenuate the neutron beam, and to allow for loading and unloading. Based on the modeling results, aluminum was chosen because it has the least attenuation for epithermal neutrons. Two halves of a container were machined with a cavity near the center for the powder. The halves were then welded together. A threaded screw hole on the side is used for powder loading and unloading (Figure 11). A prototype was dry-tested and successfully loaded with CeO_2 in a glove box by a radiochemist. Next steps were to load it with ^{233}U and confirm that it did not leak. When the holders are in use for NRTA or gamma ray measurements, they will be placed in a secondary containment (likely a mylar or polyethylene bag).

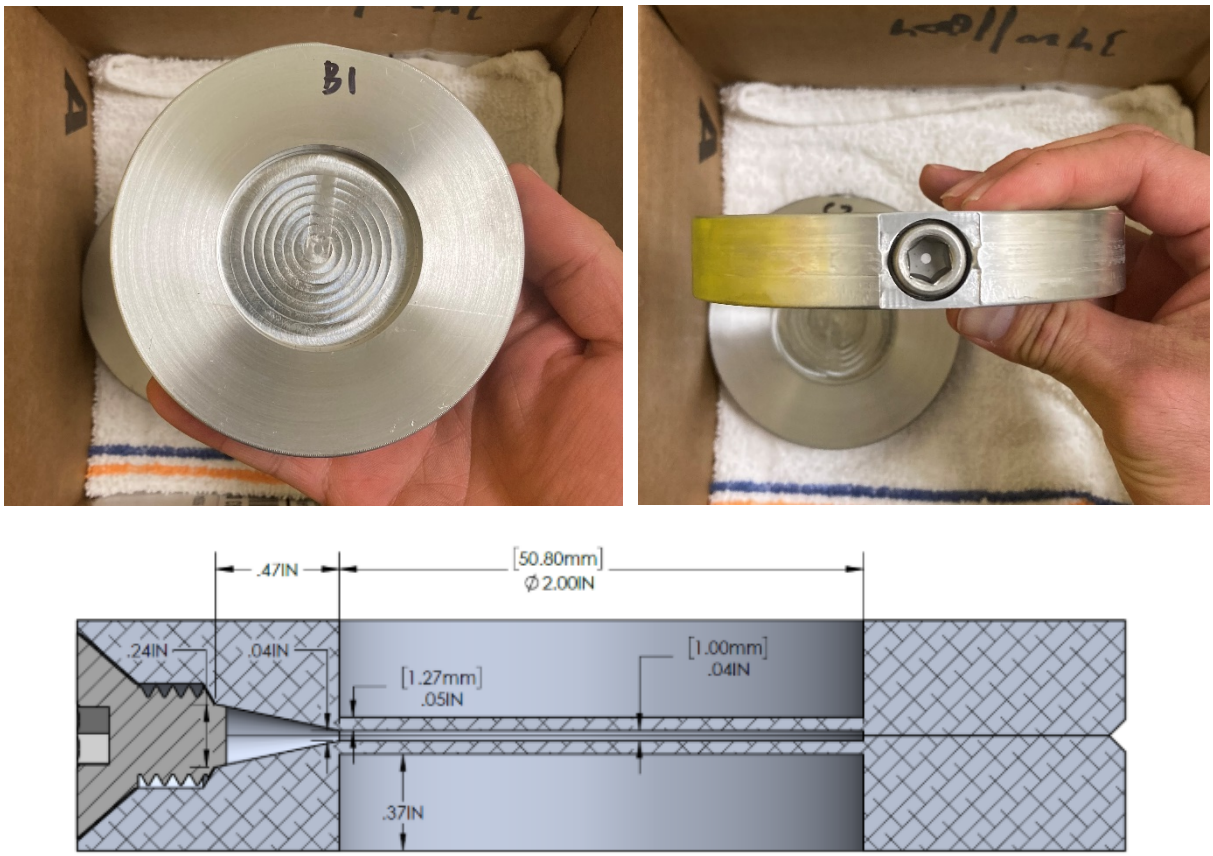

Figure 11. Photographs of a custom sample holder (top). Aluminum sample holder for ^{233}U powders (bottom). Two sides are welded together and a port at left allows filling holder. Note that the final design used a path length of 1.2 mm.

3.4 New Collimators

New collimator inserts that fit within the existing neutron shield were made to accommodate smaller sample sizes (ø50 mm). These reduce on-axis neutrons from streaming around the sample edges to the detector, which would decrease signal to noise in the TOF spectrum resonances. Collimators with diameters of 48 mm and 42 mm were fabricated. Additionally, a plug that completely covers the opening was made. This allowed background studies to be completed (i.e., determining magnitude of background that makes it through the shield). A rendering of the new collimator insert is shown in Figure 12. A photograph of all the new inserts and the original IVAC collimator is shown in Figure 13.

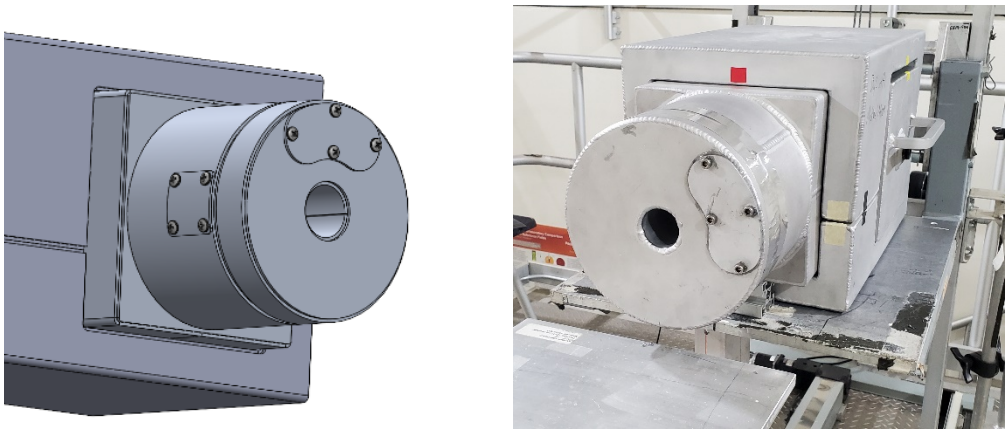

Figure 12. Rendering (left) and photograph (right) of a new collimator insert with ø48 mm opening. The hollow chambers are filled with B_4C powder to shield thermal neutrons.

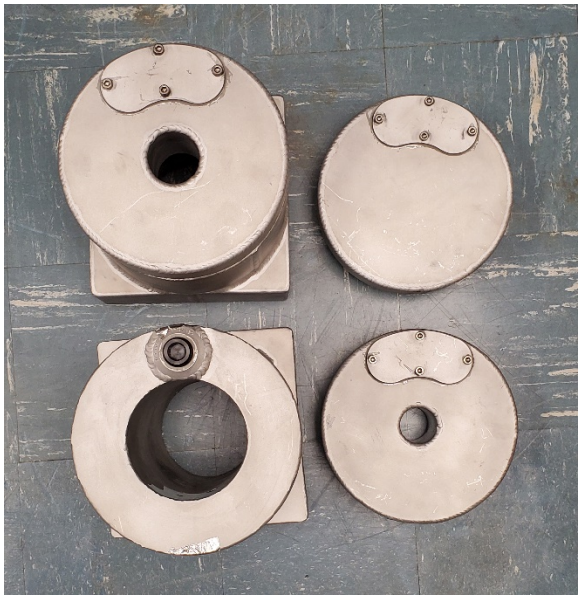

Figure 13. Photograph of the set of collimator inserts. Clockwise from top left) are ø48 mm diameter collimator on new insert holder, plug insert, ø42 mm collimator insert, and original IVAC collimator for larger samples.

This page intentionally left blank.

4.0 Detector Development

4.1 Detector Requirements

The detector for this measurement must meet several key requirements: the ability to detect epithermal neutrons in the energy range of interest, have better than 1-μs timing resolution, and have low gamma ray sensitivity (or good ability to discriminate neutrons from gamma rays). As is often the case, trade-offs exist within each detector type, and the perfect detector does not yet exist for this application. The detector, its housing, and associated readout components should also have a minimal amount of hydrogenous material to reduce neutron scattering (and resulting blurring of the TOF spectrum). Prior detector development for IVAC will be leveraged as appropriate. Gamma ray sensitivity and discrimination capabilities become key parameters if measuring irradiated or otherwise high-activity samples.

The isotopic composition, amount of the sensitive material of the detector, and ability of neutron capture reaction products to generate signal within the medium determine the detection efficiency. Figure 14 shows the cross section for various epithermal-sensitive materials for typical detector configurations. The time resolution comparison is most helpful across different classes of detector. Scintillators, in general, exhibit a very fast rise time (~1 to 50 ns). Gas-based detectors, on the other hand, are relatively slower to respond (~100 to 500 ns) due to the relatively slow ionization process. Other practical considerations are commercial availability and ease of integration. Potential options are discussed below.

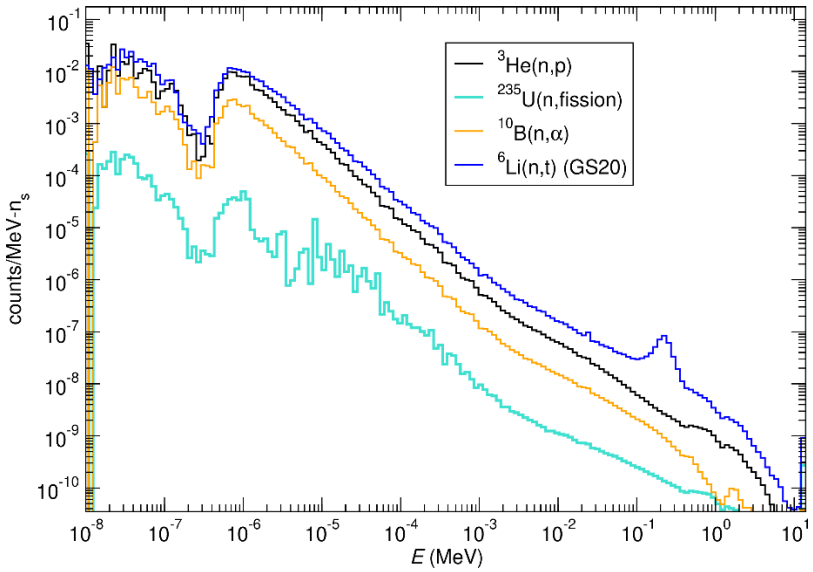

Figure 14. Modeled efficiencies for a subset of the selected detectors.

4.2 Detector Survey

The team performed reviewed recent detector literature, a commercially available detectors, and a detector survey performed on the IVAC product to identify best options for NRTA safeguards applications. Detectors that would require large development efforts (i.e., low TRL) were noted in the survey but not included for potential integration. Some recent work examined the ability of select neutron detectors to operate in high gamma radiation fields up to 700 R/hr, consistent with dose rates from small samples from MSRs (Sagadevan et al. 2021). In this recent work, the

authors compared a ^{3}He proportional counter, a custom 10B plate-based detector called the mini high-dose neutron detector (miniHDND), and a fission chamber for detection of thermal neutrons. The first two detectors had similar performance up to 700 R/hr, but the ^{3}H detector required setting a very high voltage threshold, which could lead to detection instability, and experienced a higher percentage drop in neutron counts at the highest gamma dose rates. The fission chamber was unaffected by the gamma dose rates but had much lower overall neutron efficiency. The miniHDND is a promising detector for some applications; unfortunately, the HDPE moderator make it likely impractical for NRTA measurements. The moderator in the detector effectively blurs the TOF spectrum by adding additional background terms. Removing the moderator might be possible, but then the neutron efficiencies would likely be similar as other 10B-based detectors. It may still be worth considering as it was designed to be less sensitive to gamma rays than typical detectors. A small number of miniHDND were made by PDT, Inc. The company is not currently producing these and the existing detectors are at Los Alamos National Laboratory.

4.2.1 ^{6}Li-Based Scintillators

^{6}Li-based scintillators operate on the principle of detecting scintillation photons produced by the (^{6}Li (n, α) ^{3}H)) reaction products resulting from an absorption of neutron by ^{6}Li. These scintillators contain lithium enriched to 90% or above in ^{6}Li to increase neutron detection efficiency. Suitable options include: Cs2LiYCl6:Ce (CLYC); (Cs2LiLa(Br,Cl)6:Ce) or CLLBC; GS20, LiF-ZnS; and lithium-sodium iodide (LNI) columnar scintillator film (Marshall et al. 2017; Nagarkar et al. 2015).

Elpasolite scintillators such as CLYC and CLLBC are reliable at detecting both gammas and neutrons and discriminating them with high accuracy. While the analog signal has a fast rise time, the signal generally requires longer charge integration time, up to 5 μs or longer, for good pulse-shape-discrimination (PSD) performance to separate gamma rays from neutrons. However, the longer pulse processing times increase the effective deadtime of the detector, reducing the maximum measurable input count rate.

GS20 is an exception because neutron detection is primarily performed via pulse-height analysis, so that long pulse processing times are not necessary. GS20 has been proven to function well in prior experimental studies at MIT (Klein, Naqvi, Bickus, et al. 2021). Due to the lack of PSD capability, the GS20 scintillator is susceptible to false neutron detection events in presence of high-energy gamma ray field (> 1.5 MeV). To properly characterize GS20 detector performance in the presence of high-energy gamma fields, it is important to understand the effect of gamma events. For gamma-only sensitivity study, the GS30 scintillator, depleted to < 0.01% in ^{6}Li, can be used to selectively characterize the effects of gamma-only interactions in presence of neutrons. With the ^{6}Li concentration nearly four orders of magnitude lower in GS30, it is virtually insensitive to neutrons compared to GS20.

LiF-ZnS (e.g., EJ-420) is an attractive option given its fast decay time (~ 200 ns). LiF-ZnS is commercially available in two common forms: LiF + ZnS phosphor embedded in plastic scintillator matrix, and a thin, film-based phosphor. The inclusion of plastic matrix is undesirable due to the competing process of neutron absorption on hydrogen. The absorption on hydrogen not only reduces the detection efficiency, but it also generates additional gamma background via prompt gamma emission of 2.2 MeV. Plastic scintillators in general are thus not well-suited for this application. The film-based option is limited in thickness of up to 500 μm due to self-absorption of light by the phosphor, limiting the overall detection efficiency. This low-efficiency issue is the same for other neutron imaging screens (e.g., Scintacor's NDfast screen).

LNI is a relatively new material that has been used for thermal neutron radiography. It can be grown in large sizes and up to 1 mm thick. It has a very high lithium content, and the columnar structure preserves spatial resolution as detector thickness increases. It also has good pulse shape discrimination and a high gamma-equivalent neutron peak (4.1 MeV) (Nagarkar et al. 2015). These are big advantages compared with GS20. Its main downside compared to GS20 is that it is significantly slower (~2000 ns vs. ~100 ns decay times for slowest components).

4.2.2 Helium-3 Proportional Counter

Depending on the physical dimensions and gas mixture, ^{3}He proportional counters have a rise time of 300 to 500 ns. A higher-efficiency detector can be constructed by increasing the gas pressure. The readout is simplified via the use of commercially available charge-sensitive pre-amplifiers that are attached directly to the ^{3}He tube. The pre-amplifier is an all-in-one device consisting of high-voltage generator, front-end analog pulse processing unit, a pre-amplifier, and a digital pulse output encased in a compact housing attached directly to end of the tube. An advantageous feature of ^{3}He for this application is its extremely low sensitivity to gamma rays, and a simplified readout and pulse-processing scheme.

4.2.3 Fission Chamber

A fission chamber consists of a thin layer of special nuclear material along the inner wall of an ionization chamber (typically a sealed aluminum or stainless-steel tube). A common choice of active layer is HEU (> 90% ^{235}U). Fission chambers operate on the principle of gas ionization resulting from the energy deposited by fission fragments. The analog pulse resulting from the ionization is read out in a manner similar to ^{3}He proportional counters. The rise times is within the range of 120 to 170 ns. These chambers are attractive due to their relatively high neutron absorption cross section at specific resonance energies depending on the active detection layer (i.e., ^{233}U, ^{235}U or ^{238}U); however, the extremely thin detection layer results in lower detection efficiency. The fission chambers are practically insensitive to gamma rays.

The advantage of fission chamber is that it enables a unique measurement otherwise difficult to conduct with other detector types. Depending on the special nuclear material makeup of the fission chamber (^{235}U, ^{238}U, etc.), a more direct presence measurement can be conducted. Evaluating this aspect of fission chamber will be beneficial in understanding their utility for this application.

4.2.4 Boron -10 Lined Proportional Counter

Like fission chambers, ^{10}B-lined detectors consist of thin layer of $^{10}B_4C$ along the inner wall of an ionization chamber. The reaction products (alpha and ^{7}Li), resulting from the neutron absorption by the ^{10}B nucleus, ionizes the gas. The read-out mechanism is similar to that of a ^{3}He proportional counter.

Currently available commercial options include the traditional design (single tube, large volume) described above. The timing response of this design is ~50 ns to 250 ns. The other option consists of small-diameter tubes packed together inside a single tube. The latter design is commercially known as boron-coated straws (BCS). BCS can provide position information by recording the analog signal at both ends of the tube. The faster time response (~50 ns) and pulse timing measurements can provide event position within the tubes. The BCS design is selected for its faster time response. ^{10}B-based detectors also have low sensitivity to gamma rays and provide favorable neutron absorption cross-section in the energy range of interest.

4.2.5 Neutron-Sensitive Microchannel Plate

Neutron-sensitive microchannel plates (MCPs) consist of an array of extremely fine glass channels (~ 3 to 4 microns wide) embedded with ^{10}B. The reaction products, defined in Section 4.2.4, give rise to primary and secondary electron cascades in sufficient quantities to convert electrons to light via a phosphor screen. A charge-coupled device (CCD) or complementary metal oxide semiconductor (CMOS) camera is used to detect the visible light from the phosphor screen. These systems provide high spatial and timing resolution. At 100 ns timing resolution, they provide an option for faster readout. Boron-impregnated MCPs are made by just one company (NOVA Scientific), and at the time of the research team's survey, it was being purchased by Photonis. A German company, ProxiVision GmbH, integrates MCPs into a neutron camera system with 40 mm active diameter and 50 µm spatial resolution ("MCP Neutron Detector") MCPs are sensitive to gamma rays because they typically have high lead content in the glass. Some improvements to neutron/gamma discrimination have been explored by reducing the gain of the MCP and using pulse height data (Tan et al. 2022). However, neutron discrimination would likely be impossible in high gamma backgrounds due to pulse pileup. Since these had an indefinite lead time of over a year, the research team did not evaluate these further.

4.2.6 TPX3CAM

A TimePix3-based neutron camera, the TPX3CAM, is a system commercialized by Amsterdam Scientific Instruments (ASI). It includes a scintillator or phosphor screen mirror-coupled to an MCP, the output of which is lens-coupled to a TimePix3 sensor. The optics allow for variable field of view and image spatial resolution. The TimePix3 chip is event-driven and has very high count-rate capability and timing resolution. An earlier MCP's read out by TimePix sensors has been demonstrated to work in high gamma fields with shielding mitigations (600 R/hr) (Tremsin et al. 2018). The TPX3CAM has recently been demonstrated for energy-resolved neutron imaging of nuclear fuel slugs (Adrian Simon Losko et al. 2022). One intriguing feature of this system is the ability to discriminate neutron and gamma ray interactions via their spatial and time distribution of scintillation light (A. Losko et al. 2021). This has been demonstrated with thin $^{6}LiF;ZnS$ scintillators, which do not have good efficiency for NRTA. This functionality has not yet been tested with GS20. Thicker (~5 mm) GS20 would also provide poorer spatial resolution than the thin screens, but imaging and spatial resolution are not currently the focus of our NRTA measurements. It would be interesting to test a TPX3CAM with GS20 or columnar LNI scintillators. The timing information collected by TPX3CAM, which digitizes each scintillation decay, could be used to discriminate neutrons from gamma rays in LNI. Purchasing a system was cost-prohibitive, but it can be rented for several months for evaluation purposes.

4.3 Detectors Selected for Evaluation

Detectors for further evaluation and comparison were selected based on the performance properties, cost, and availability. The down-selected options include GS20, ^{3}He proportional counter, ^{10}B based detectors, and fission chambers. CLYLC and LNI detectors are still being considered.

A comparison of the down-selected options is shown in Figure 14, which shows the simulated counts in each detector as a function of energy. The detector options were constrained to similar geometries to provide a direct comparison. The GS20 glass scintillator is quite efficient at detecting neutron given its high ^{6}Li atom density. The ^{3}He at 3 atm performs nearly as well as GS20 below 10 eV, with the added benefit of little to no gamma sensitivity. Further studies

suggest that 10 atm of ^{3}He would moderately outperform the GS20 glass scintillator. The ^{10}B proportional counter is expected to be ~30% less efficient than that of the modeled efficiency after factoring the escape fraction of reaction products responsible for registering a count. The fission chamber enables a unique measurement approach, but the thin detection layer makes it an impractical solution with a low detection efficiency. A suitable fission chamber and required readout hardware are readily available at PNNL, therefore limited experimental evaluation will be conducted for comparison purposes.

The following detector designs were selected for further evaluation.

- **GS20 and GS30.** Two variations of lithium-based scintillator detectors have been constructed to understand the competing processes of gamma background and neutron efficiency. The designs include a ø50 mm x 5.0 mm thick GS20 and GS30 coupled to a ø76 mm PMT (Figure 15). A 2.5 mm thick GS20 detector is also available at PNNL and will be tested. Modeling at MIT has shown that reducing the GS20 thickness greatly reduces sensitivity to high energy gamma rays that may be mistaken as neutrons.

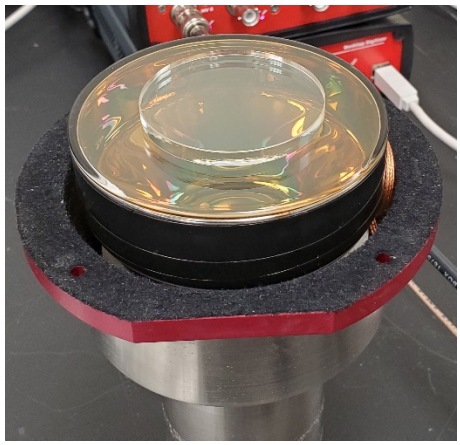

Figure 15. Photograph of GS20 coupled to a PMT.

- **^{3}He proportional counter.** Two variations of a ^{3}He detector have been finalized to study the neutron detection efficiency and timing as a function of gas pressure. The designs include ø25.5 mm x 76.2 mm active length tubes with the gas fill pressure of 4 and 10 atmospheres (Figure 16).

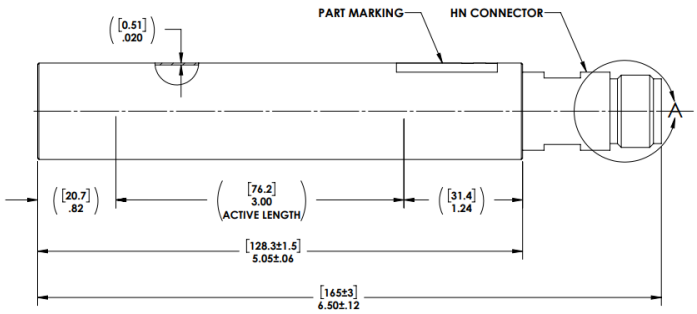

Figure 16. Schematic of the ^{3}He detector design.

- **Fission chamber.** A fission chamber that is currently available at PNNL will be evaluated for timing characteristics and detection efficiency. The design specifications include ø25.4 mm x

127 mm active lengths. The active layer consists of ^{235}U enriched at 93%, amounting to 13 mg of ^{235}U. This is one of the highest efficiency designs and the most immune from gamma ray interactions. However, its efficiency is two to three orders of magnitude lower than the other detectors, meaning that measurement times may be impractical for most scenarios. The research team only plans to make minimal measurements with fission chambers.

- **^{10}B-lined proportional counter.** Two ^{10}B designs have been selected for experimental evaluation. One design includes a traditional ^{10}B-lined proportional counter of ø25.4 mm x 107 mm of active length. This design is readily available from the manufacturer. The other design comprises seven boron coated copper straws enclosed within a tube of ø25.4 mm x 76.2 mm active lengths with an integrated pre-amplifier. The active detection layer consists of 1.3-micron $^{10}B_4C$ layer.
- **CLYC.** MIT plans to study trade-offs with count-rate capability and neutron discrimination performance for NRTA with a CLYC detector being procured on the IVAC project.
- **LNI Screen.** PNNL is attempting to procure an LNI screen from RMD, Inc. This material has good PSD performance, has slightly faster decay times than CLYC/CLLBC, and is grown in columnar structure. The columnar nature channels light from an individual interaction so spatial resolution is preserved, which could be useful for proof-of-concept NRTA radiography measurements. The material is typically grown in a maximum of 1 mm thickness, which may be helpful for reducing gamma ray sensitivity. By weight, it has more lithium than GS20.

The detector time response, neutron detection efficiency, and neutron response in the presence of large gamma fields of each detector will be evaluated experimentally. The research team will compare the relative time responses and efficiencies to rank each detector. While both the timing and efficiency are important criteria for this application, it is expected that the detector with faster time response will perform better overall. Lower detection efficiency can be compensated by using multiple detectors.

The research team also plans to perform NRTA measurements with these detectors in large, controlled gamma ray fields. This is possible in the facility where the NRTA experiment is set up by bringing in high-activity gamma ray sources via pneumatic tubes. These can create calibrated dose rates and the research team aims to test up to 500 R/hr (and to determine the limit for each detector below that rate). Furthermore, the research team will investigate gamma mitigation strategies. For instance, some lead shielding can be used between the detector and sample with minimal impact on the neutron transmission.

5.0 Measurements and Analysis

5.1 Characterization of ^{233}U Oxide material

On April 26, 2022, the research team took a sample from Radioactive Materials Tracking (RMT) item #39, for gamma spectroscopic analysis. The item was opened in the Radiochemical Processing Laboratory (RPL) room 410 glove box and gravimetrically sub-sampled into a 3 mL Savillex vial depicted in Figure 17. A mass of 60.3 mg was transferred to the vial.

Figure 17. Photographs of the ^{233}U powder sample (left)and a dilution aliquot (right).

The sample was counted at a stand-off distance of 20 cm using detector G, an Ortec 40% relative efficiency HPGe detector, in RPL. The measured activity was determined to be 1.483e7 Bq +/- 5.4% or 41.6 mg of ^{233}U, not in agreement with the gravimetric mass when treated as U_3O_8 (51 mg). This indicates a lower overall uranium fraction. Next, the research team dissolved the sample and prepared two dilution aliquots for coincidence spectroscopic analysis. A photograph of the coincidence system is shown in Figure 18.

The sample was taken to RPL room 506 and dissolved in glove box unit #1 using concentrated nitric acid. The dissolved sample is shown in the right side of Figure 17. Once dissolved, the sample was opened in a fume hood and diluted into three vials. An aliquot of 100 µL (0.141 g) of the stock was transferred into a vial containing 0.9022 g of DI water to obtain 1.e6 Bq of ^{233}U. A fraction of this stock was placed in 9.9 mL of Ultima Gold A/B to prepare a 1.e5 Bq sample for testing. A second 10x dilution was performed and 100 µL of the second dilution (0.106 g) was taken and placed into 9.9 mL of Ultima Gold A/B for charged particle coincident gamma-gamma counting at 1.e4 Bq. The sample was counted for ~1.5 days and the particle split data are shown in Figure 19.

Based on the charged particle coincident split spectra, there were no indications of ^{235}U or ^{238}U in the sample material. The observed 185 keV gamma was consistent with a weaker line of ^{229}Th in the alpha-gated gamma spectrum. Figure 19 depicts the charged particle (CP) split spectrum within this region.

Figure 18. Photograph of the coincidence system in RPL.

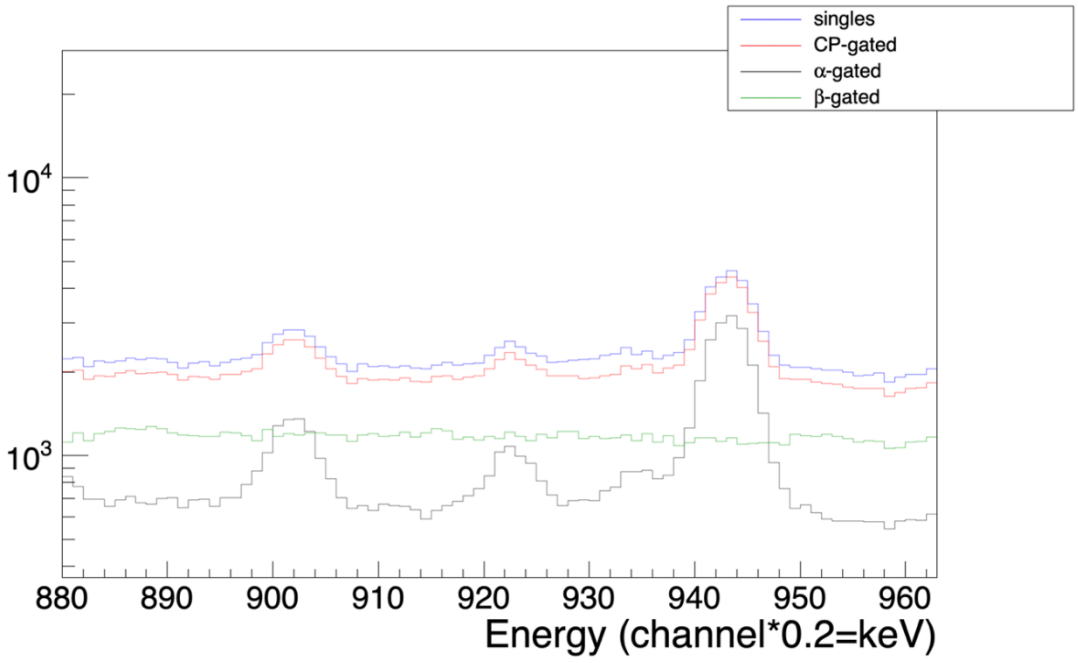

Figure 19. Spectra with singles and different coincidence gating from charged particle interactions in a liquid scintillation vial for the 129 keV region.

There was no observable 1001 keV gamma in the beta-gated and ungated spectra, as shown in Figure 20.

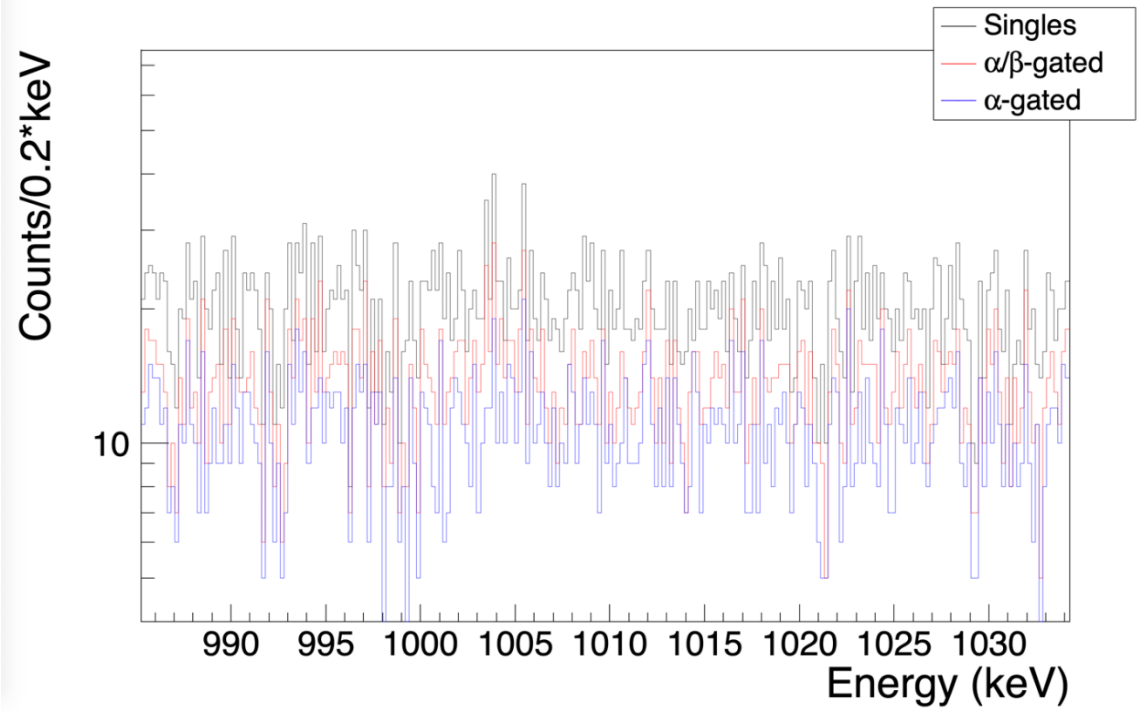

Figure 20. Spectra for singles and coincidence gating for the 1001 keV region.

Gamma detection efficiency at 1001 keV is quite low and the ^{238}U daughter ^{234m}Pa branching ratio to the 1001 keV gamma is quite low, increasing the minimum detectable concentration (MDC) relative to other features like the 92.5 keV feature of ^{234}Th. The 92.5 keV gamma-line was observed using charged particle gating as shown in Figure 21.

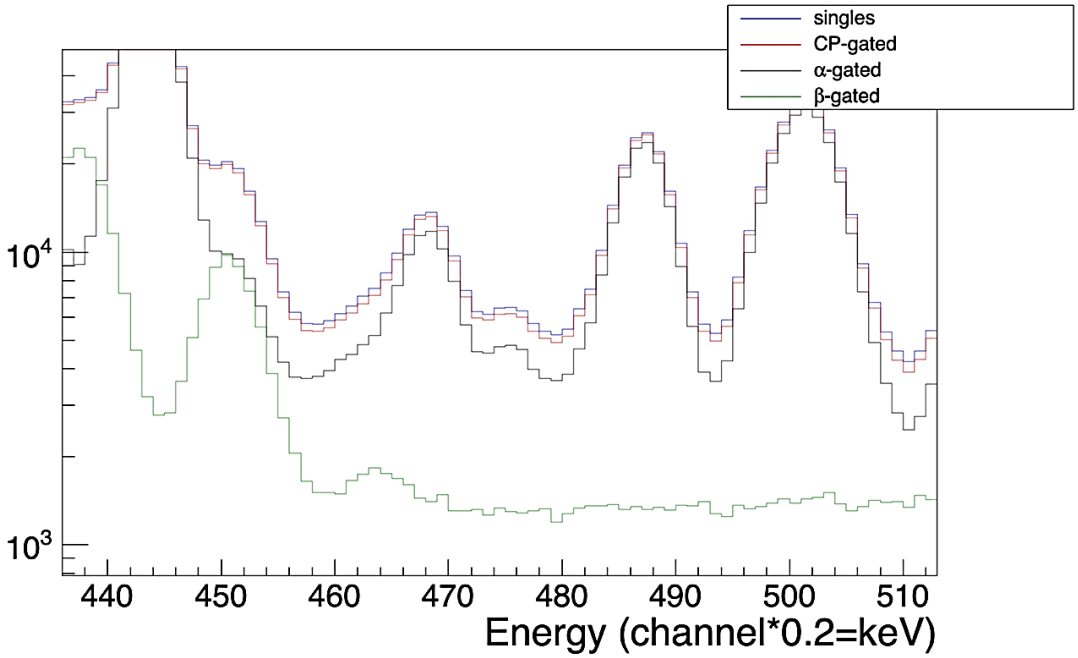

Figure 21. Spectra for singles and coincidence gating for the 80-100 keV region.

On further inspection, however, the activity as measured using at 92.5 keV and using the ^{213}Bi coincident feature at 293-807 keV were consistent with ^{229}Th.

The few remaining features identified in the sample were ^{241}Am and ^{234}U. On close inspection, the 59.5 keV gamma is quite prominent and clearly associated with an alpha-emitting source as shown in Figure 22. The ^{229}Th daughter product of ^{233}U does emit a gamma ray at 59.3 keV. The activity estimate of ^{229}Th derived from this feature is a factor 100 larger than the measured activity of ^{229}Th using 15 of the 21 gamma-lines used to measure ^{229}Th. Based on a search of the available radionuclides that emit an alpha and gamma in coincidence, ^{241}Am is the most likely identification.

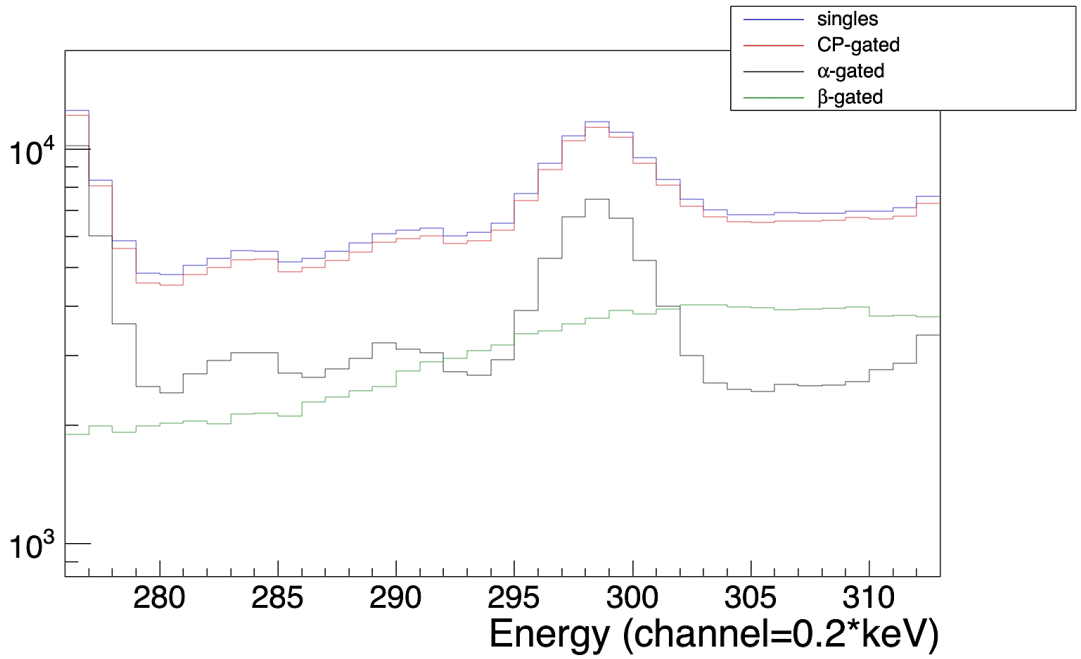

Figure 22. Spectra for singles and coincidence gating for the 60 keV region.

A review of possible ^{234}U contamination in the sample was also performed. This radioisotope is very long-lived and is most commonly observed in the enrichment process of ^{235}U but also could be present from ^{233}U(n,γ) reactions accumulated over the irradiation production of ^{233}U from ^{232}Th capture. Because ^{233}U and its daughter ^{230}Th are both very long-lived, the most prominent gamma features that could be observed are the 120.9 and 52.3 keV gamma-lines of ^{234}U. Unfortunately, both regions of the singles alpha-gated singles spectrum are quite busy and indicate features potentially attributable to ^{234}U as shown in Figure 23.

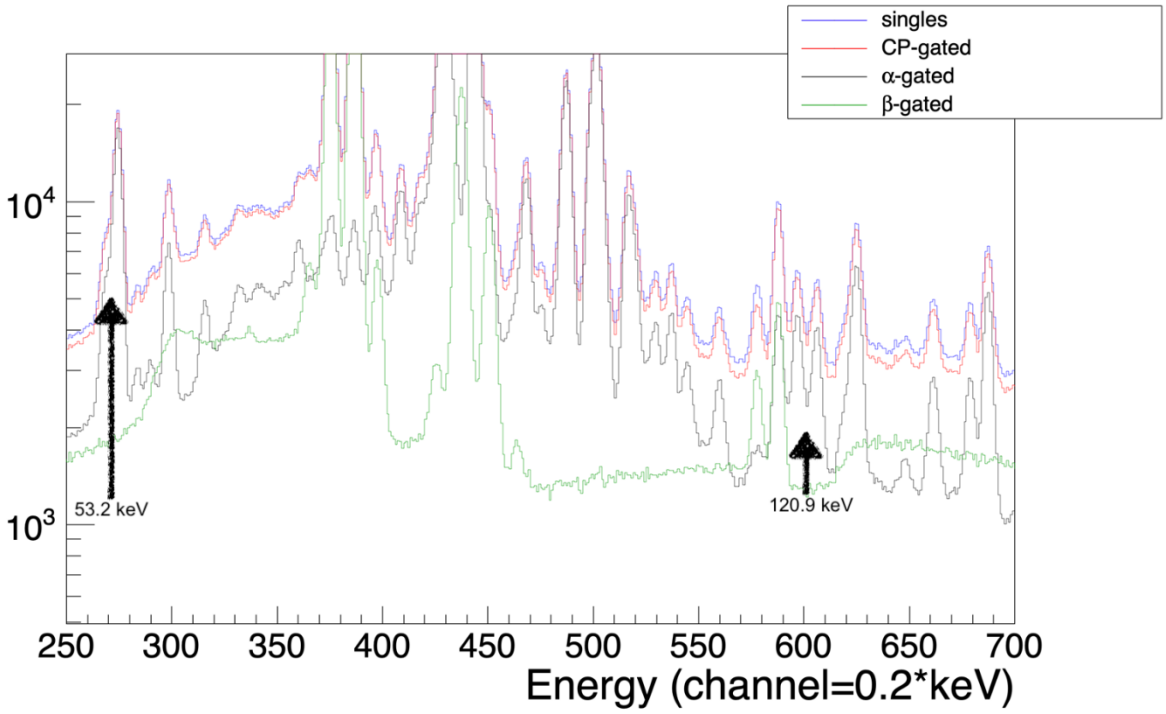

Figure 23. Singles and coincidence gated spectra for the 50-130 keV region with arrows pointing to ^{234}U peaks.

However, the alpha-gated coincidence plane in this region does not support quantification or significant presence of ^{234}U as shown in Figure 24. The results for all assayed isotopes are given in Table 2.

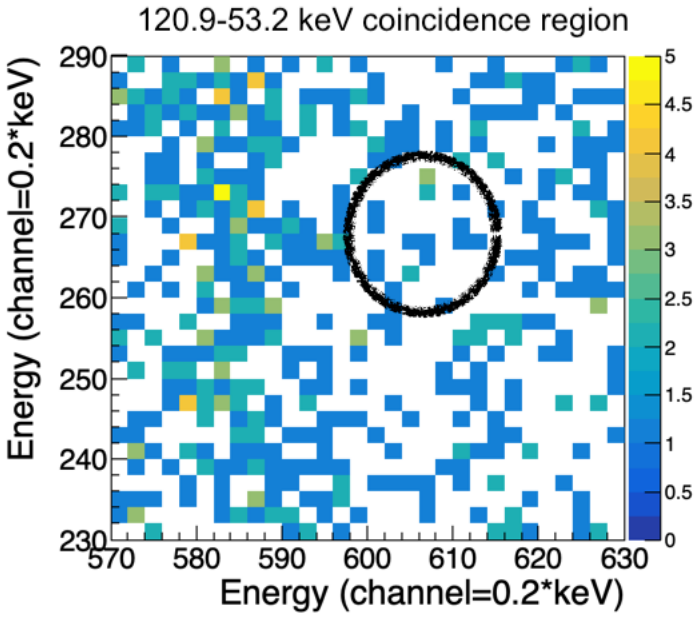

Figure 24. Coincidence plane spectra for 50-130 keV region.

Table 2. Isotope assay results from coincidence analysis.

Isotope	Specific Activity (Bq/g U_3O_8)	+/- %
Tl-208	4.95e5	2.33
Tl-209	8.20e5	3.59
Bi-212	1.35e6	2.59
Pb-212	1.52e6	3.43
Bi-213	1.23e6	2.47
Bi-214	BKG	
Pb-214	BKG	
Fr-221	1.57e6	4.15
Ra-224	1.52e6	3.49
Ac-225	#POOR AGREEMENT	
Ra-225	5.86e5	30%
Th-228	1.52e6	2.85
Th-229	1.24e6	10.4
U-232	**assume eq. Th228	
U-233	2.46e8	5.5
Am-241	4.36e4	4.0

Based on the secular equilibrium of ^{233}U and ^{229}Th, the best estimate of the last chemical separation assuming quantitative separation of thorium and uranium is 50.64 (+/-5) years. Given the age of the ^{233}U, it is safe to assume the ^{232}U is in equilibrium with the ^{228}Th. Using the ^{228}Th activity as a surrogate for ^{232}U, the ^{233}U purity is 99.9996% of the uranium material with a small quantity of ^{241}Am present.

In addition to the analysis described above, we also made measurements with CZT detectors. Approximately 1 kBq of ^{233}U was deposited and dried on a flat substrate and counted with two M400 CZT detectors (H3D Gamma, Inc), and later with a single GRA1 CZT detector (Kromek, Inc.). The M400 detector setup is shown in Figure 25. Coincidence data were taken but has not yet been analyzed.

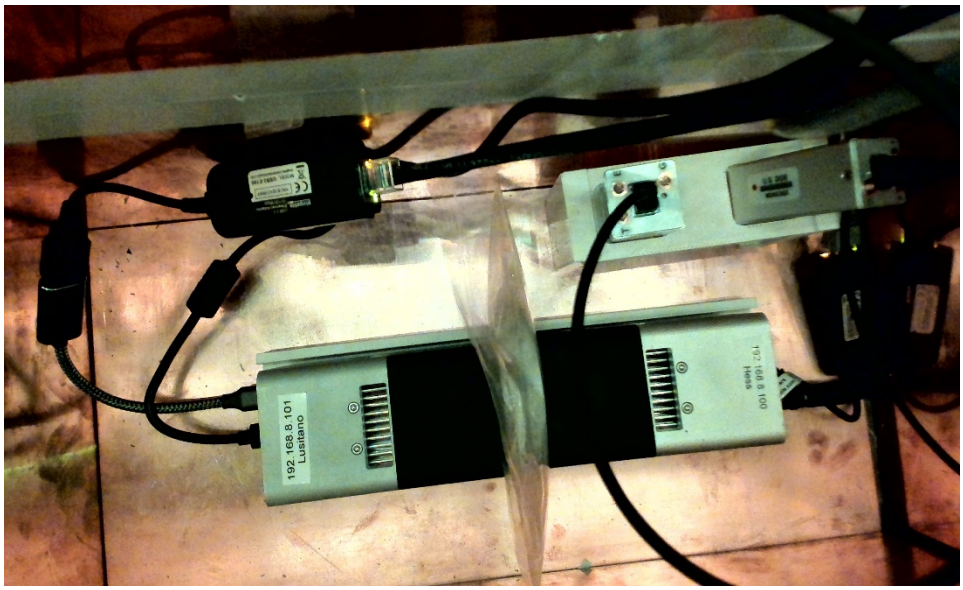

Figure 25. Photograph of two M400 CZT detectors sandwiching an AC mount sample with dried ^{233}U solution.

Example spectra for M400 and GR1A detectors are shown in Figure 26. The live time for M400 was 909740 seconds (~10 days); the live time for M400 background was 614087 (~7 days); and the live time for GR1A was 615378 seconds (~7 days). The CZT crystal is considerably smaller in the GR1A compared with the M400.

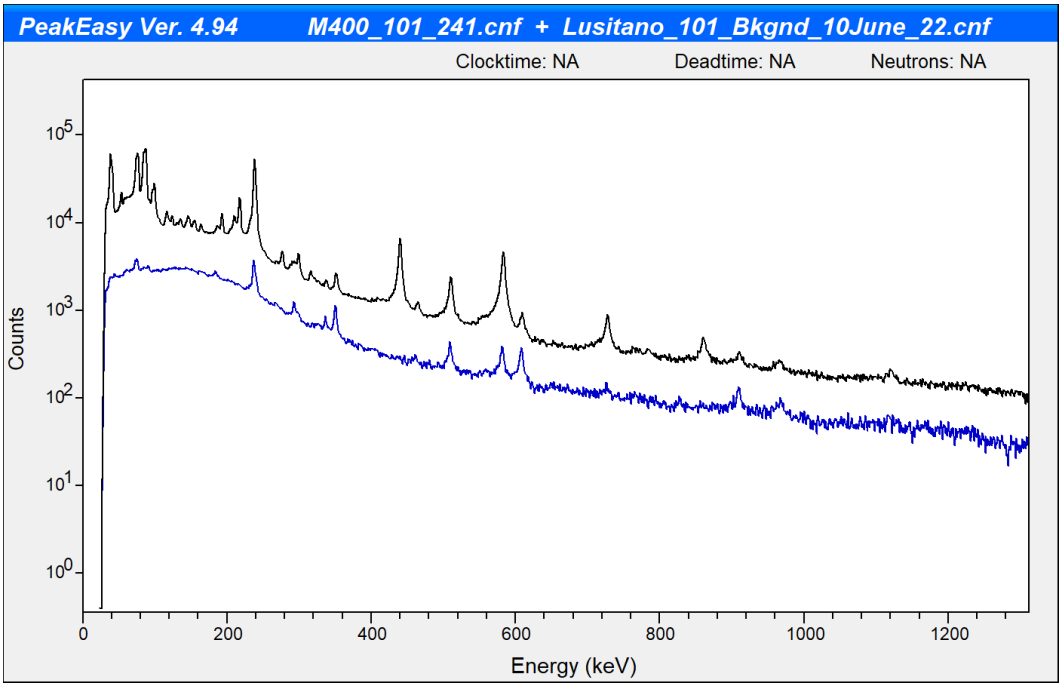

Figure 26. Example spectra for M400 (black) and GR1A (blue) detectors.

5.2 First ^{232}Th Measurements

First, the research team completed NRTA measurements on a thorium source. The thorium source (metal, 3 mm thick) is shown in Figure 27 with a source-to-detector distance of 2.035 m. Measurements were made for one hour with the source, one hour for open beam (to calculate neutron transmission), and two hours for a passive background. In IVAC measurements, passive backgrounds were typically not a concern for most sources. For high gamma-emitting sources like those expected in thorium fuel cycles, this is an important step to remove a constant background term of high energy gammas that may be misclassified as neutrons (especially in the GS20). For both measurements, a 2.00 mm thick cadmium target was present on-axis to reduce thermal neutron wraparound.

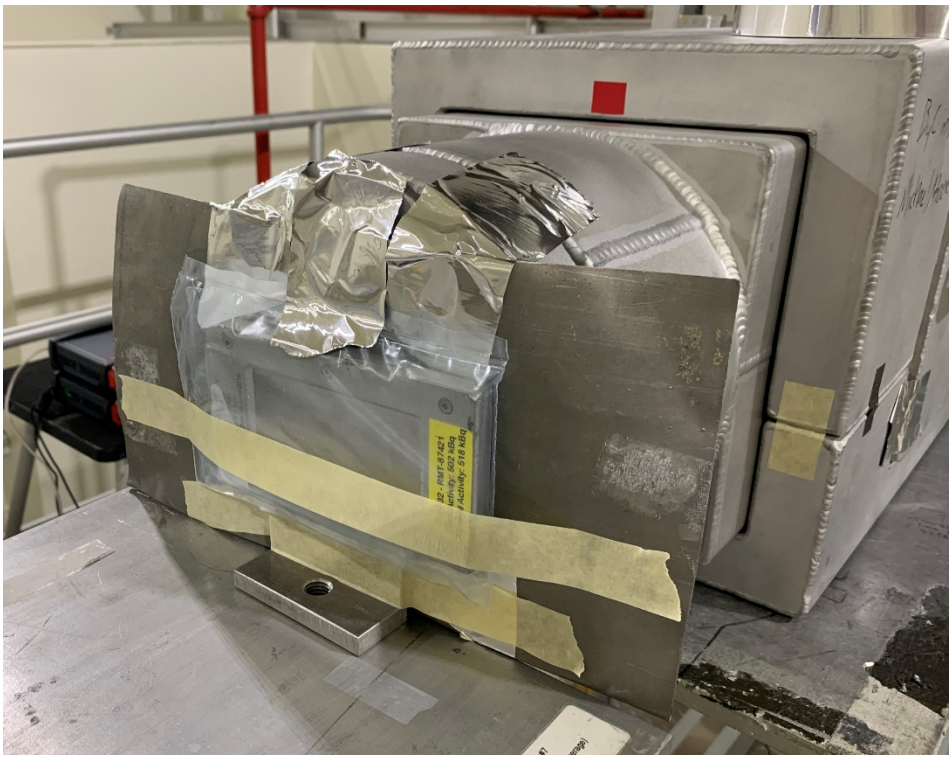

Figure 27. Photograph of the NRTA measurement setup with the ^{232}Th source target. A cadmium sheet is visible behind the source.

Background in the ^{6}Li glass scintillator can come from several different sources and a background model was developed to account for off-axis room background (constant), on-axis target-dependent background (variable), passive background from spontaneous decay in the thorium (*Th*), and increased active background due to the presence of hydrogenous material (*H*):

$$C_{bg}^{tot} = C_{const} + w_{trans}^{var} \cdot C_{var} + C_{Th} + C_{H}$$

where $w_{trans}^{var} = e^{-n \cdot \sigma_{tot}(E^{offres}) \cdot x}$ and n is atomic density, $\sigma_{tot}(E^{offres})$ is the total neutron cross-section at off-resonance epithermal neutron energy, and x is the target thickness.

These contributions were determined empirically using a set of thin- and thick- resonant targets to determine the different background contributions. The relative magnitudes of each of these

four terms for the Th target is shown in Figure 28 normalized to 1-μs bin width and 1-minute measurement time.

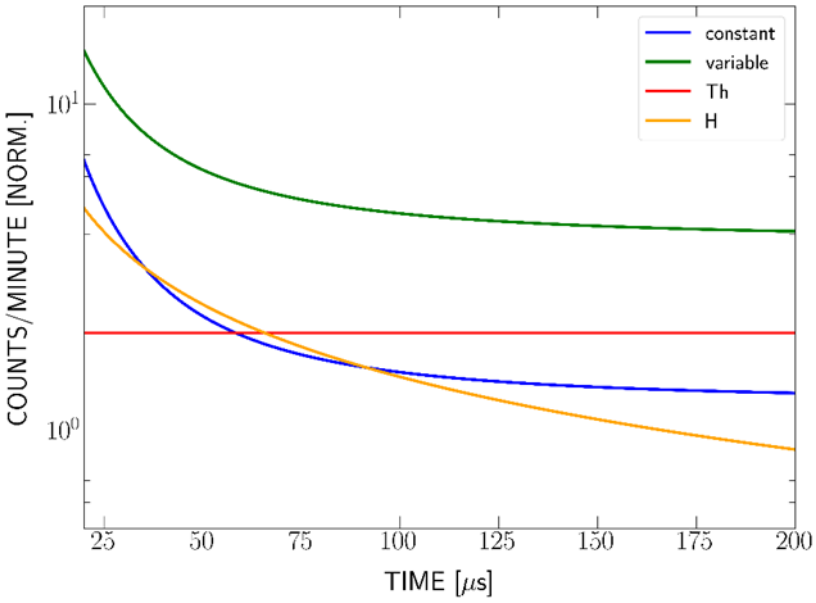

Figure 28. Background components for the neutron thorium target measurement.

The experimental transmission was calculated by correcting the target-in and target-out spectra for background and taking their ratio:

$$T_{expt} = \frac{C_{in} - C_{bg,in}}{C_{out} - C_{bg,out}}$$

This was then compared to calculated transmission spectra based on ENDF-B/VIII.0 neutron cross sections convolved with a system resolution function. The resolution function accounts for uncertainty in the neutron TOF due to the finite nature of the source neutron pulse width and the distribution in neutron moderation time. The resolution function can be approximated by a Gaussian with width σ_{res}, which was empirically determined to be approximately $0.8\ \mu s$.

$$T_{calc} = e^{-n \cdot \sigma_{tot}(E) \cdot x} * \mathcal{N}(0, \sigma_{res})$$

The comparison of experimental and calculated neutron transmission spectra is shown in Figure 29. The magnitude of the thorium dip in neutron transmission around 30 μs is due to 21.8 and 23.5 eV matches well between experiment and calculation. The thorium target was kept in a mylar bag, which was assumed to be 2.0 mil thick, but required an assumed thickness of 1.50 mm to achieve a reasonable agreement in the off-resonance neutron transmission. The deviation in off-resonance transmission after around 125 μs is likely due to an error in the background correction.

Figure 30 shows another version of the plot that shows detector counts versus time. The passive and open-beam backgrounds were removed in both figures. These initial results show it is possible to detect relevant thorium concentrations in practical measurement times. Further analysis will be done to estimate thorium mass in the field of view from this and other data. The

3 mm thorium would saturate in limit of perfect resolution, but the resolution function due to finite neutron pulse width and distribution in moderation time is convolved with the ENDF-calculated transmission (black line in Figure 29). After convolution, the now-broadened narrow resonances do not saturate, the resonance dip only going as low as 0.5 transmission.

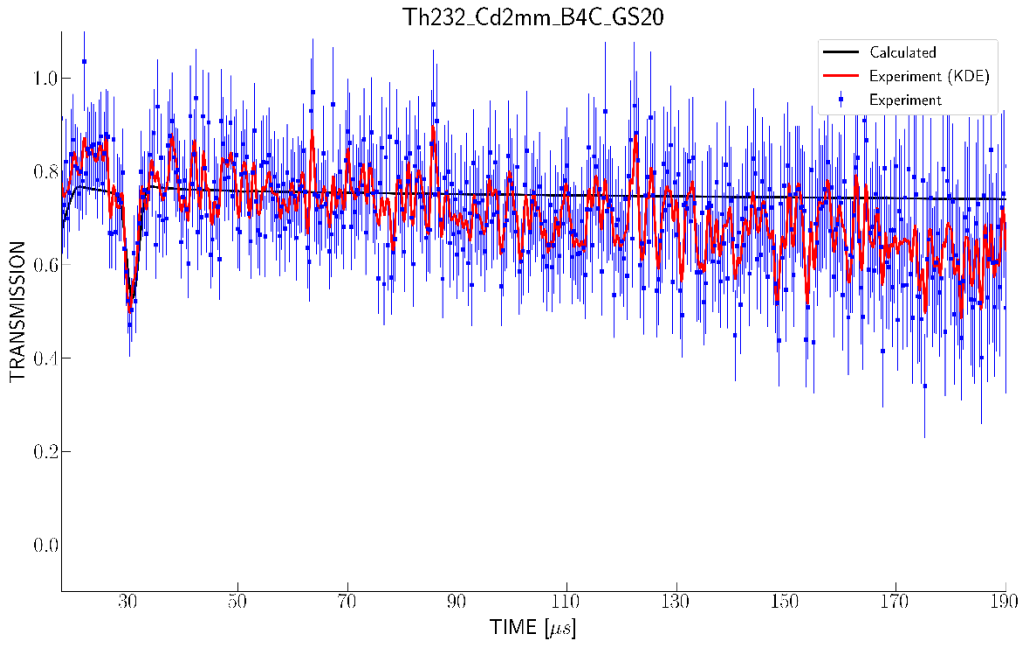

Figure 29. Comparison of calculated and experimental neutron transmission signal through a ^{232}Th target with the GS20 detector. The calculated line (black, from ENDF data and system timing resolution). The red line is the measured data convolved with a Gaussian kernel density estimate (KDE). Bin width is 333 ns.

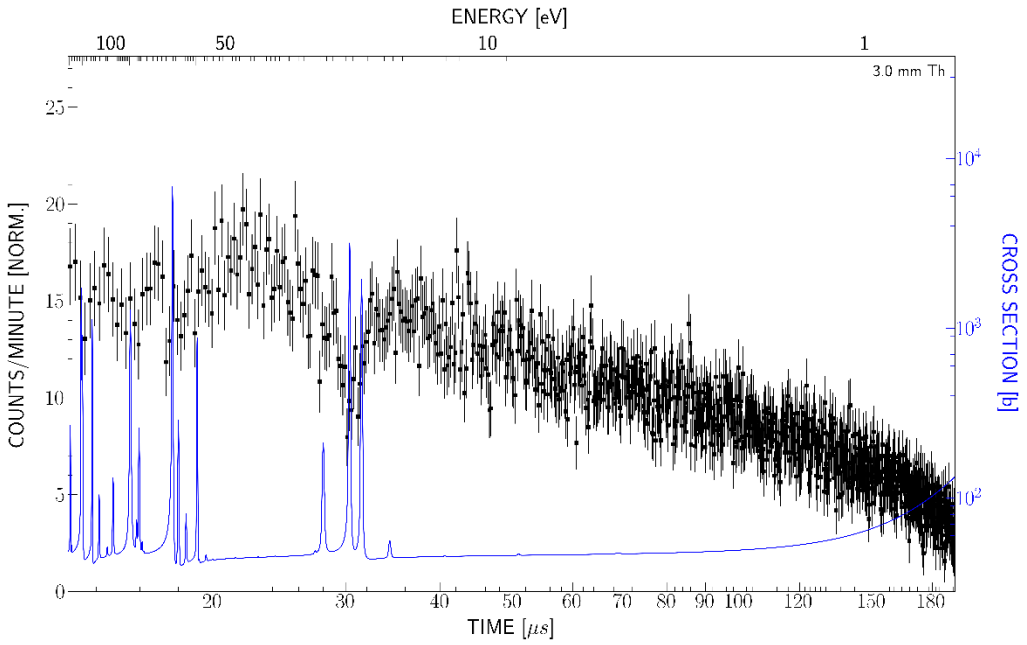

Figure 30. Plot of GS20 counts versus neutron flight time with thorium cross sections overlaid. Bin width is 200 ns.

This page intentionally left blank.

6.0 Algorithm Development

The research team is developing analysis algorithms that can be used to estimate sample isotopics from the NRTA scan. This goes one step beyond isotope identification to isotope quantification. Isotope quantification is possible because neutron resonances for isotopes of interest show uniqueness in the energies of interest for the NRTA measurements, as shown in Figure 31.

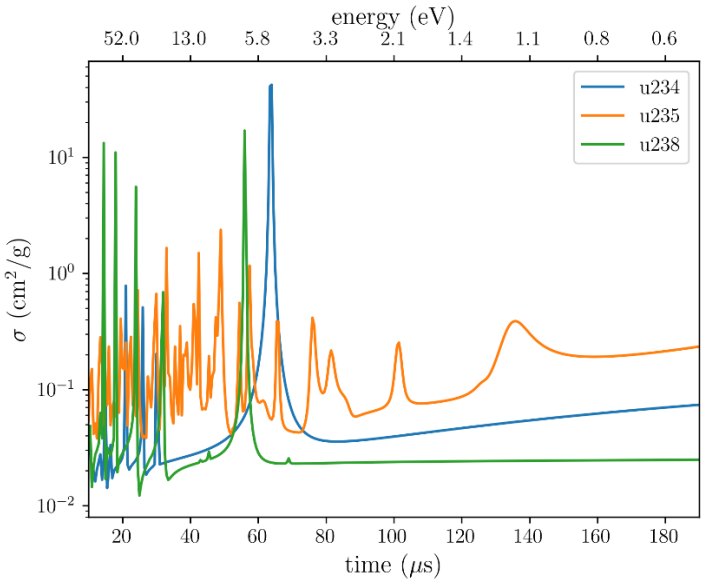

Figure 31. Uranium isotopic neutron cross sections in the time, and energy, range of interest to the NRTA measurements.

To make isotopic composition estimates, the research team is building on our previous experience with determining elemental compositions with spectral X-ray radiography data (Gilbert et al. 2014; McDonald et al. 2022). Here, the research team developed a physics model of the NRTA system and determine the isotopic composition by completing a best fit of modeled data to the observed data.

$$\vec{d}_{mod}(\vec{\rho}) = \frac{\vec{d}(\vec{\rho})}{\vec{d}(\vec{0})}$$

$$\vec{d}(\vec{\rho}) = \mathbf{C} * [\phi(t_0, \vec{\rho}), \phi(t_1, \vec{\rho}), \cdots, \phi(t_M, \vec{\rho})]$$

$$\text{where } \phi(t_j, \vec{\rho}) = \phi_0(t_j) \exp\left[-\sum_i^N \mu_i(E)\rho_i\right] + BG(t_j)$$

$$\vec{\rho}_{est} = \min_{\vec{\rho}} \|\vec{d}_{mod}(\vec{\rho}) - \vec{d}_{obs}\|^2 \quad (1)$$

The data model $\vec{d}_{mod}$ is the ratio of the attenuation with an interrogated item present $\vec{d}(\vec{\rho})$ to that without $\vec{d}(\vec{0})$. Note that the attenuation data vector is convoluted with a convolution operator $\boldsymbol{C}$ that emulates the finite temporal resolution of the NRTA system. Further, BG simulates the

background neutron flux which may be present in the system. The data vectors are composed of transmitted data $\phi(t_j, \vec{\rho})$ at times observable in the NRTA system for a given set of material densities $\vec{\rho}$. The inverse problem is then to find the best least-squares fit of the data model to the observed data, the minimum of this with respect to $\vec{\rho}$ is the estimated material composition. This optimization is done using the SciPy optimize package for Python (Virtanen et al. 2020). For this process, a set of isotopes to quantify is selected beforehand. In the future, this set of isotopes could be selected autonomously based on the location and magnitude of the dips in the NRTA system data.

As a first step to understand the feasibility of determining quantitative isotopic compositions from the NRTA measurements, a simplified data model was compared with an MCNP. The MCNP model of the time spectrum from neutron transmission through a 2-mm thick ^{233}U powder is shown in Figure 32. The MCNP model does not include a finite time resolution or a background term, which are also ignored in the physics model in making the material estimations. The forward model calculations (orange line) show very good agreement with the MCNP results. Largely, the differences seen are due to the time binning used in the MCNP model and a poor fit at longer times due to neutrons scattering before getting to the detector. Importantly, the MCNP model and forward model agreement is good at the neutron resonances over the range of interest, up to 200 μs.

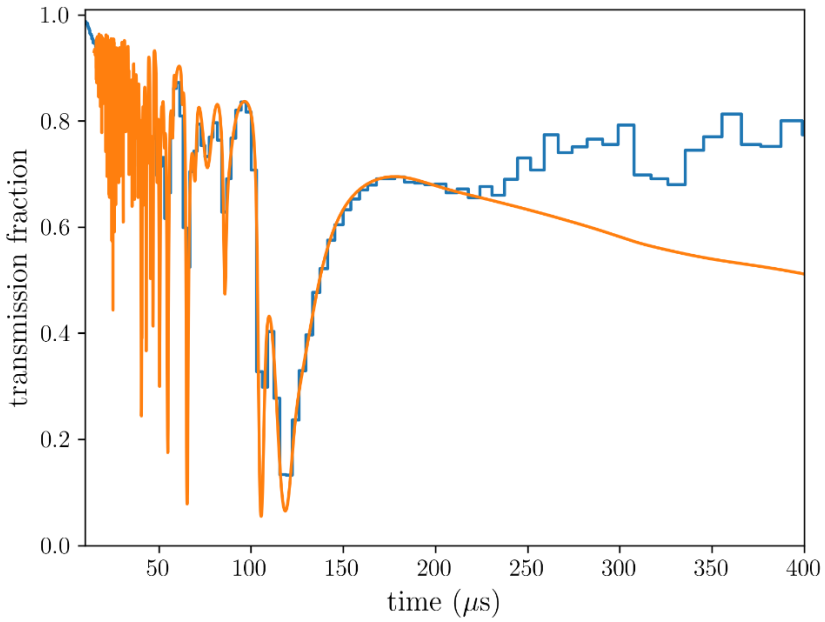

Figure 32. Comparison of an MCNP simulation of the NRTA system (blue) and the output from the initial system forward model (orange) for a 2-mm thick $^{233}UO_2$ powder.

Forward model agreement with the MCNP simulations is encouraging and indicates that the system can be modeled with simple equations. This will enable fast and accurate inverse algorithms to be used to determine the isotopic composition from the data. Next, the research team explored determining isotopic compositions from experimental NRTA data and adding realism to the physics model by using the convolution kernel to simulate finite temporal resolution. The research team tried Gaussians of differing widths and found that a kernel that resembles the neutron pulse profile (left side of Figure 33) provided the closest match between the forward model and the measured data. The data used a tungsten sample of known

composition and thickness, which is input to the physics model to generate Figure 33 (right). In this case, one of the key takeaways from fitting-by-eye is that it appears there is not a significant constant background term from neutron wrap-around, indicating the research team can represent some of the physics of the NRTA system with simple (and fast) convolutions.

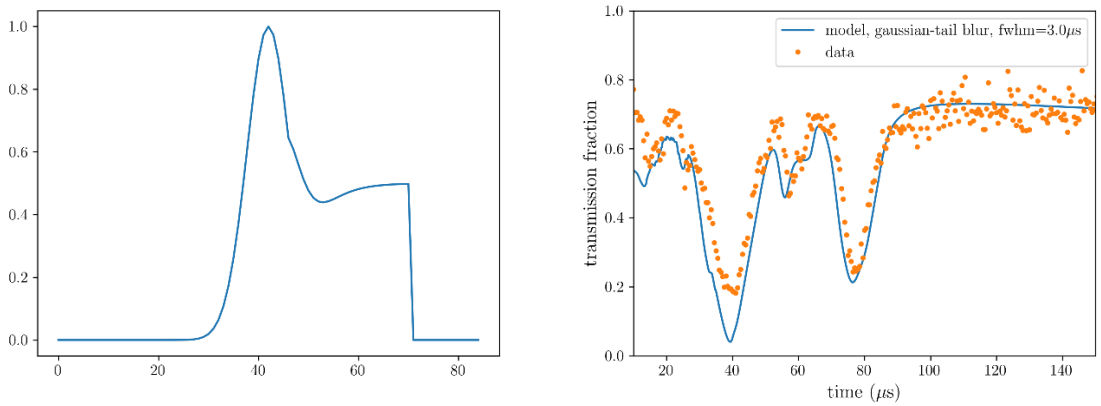

Figure 33. Pulse structure of the neutron generator (normalized intensity versus time in μs) (left). Plots of forward-model data and measured NRTA TOF spectra for a tungsten sample (right).

A pulse shape such as that shown in the left of Figure 33 is not ideal in that the blurring is wide and will make it difficult to resolve nearby dips in the NRTA data. The parameters used in running the neutron generator were updated to create a narrower and symmetric pulse profile, which is a better fit to the Gaussian curve. The research team updated the physics model and used it to estimate the uranium isotopics from measured data of a depleted uranium plate. Figure 34 shows the measured TOF spectrum and the best fit model results. The modeled resonances are somewhat deeper than the measured data, but overall, the shapes and magnitudes agree well. The output of the algorithm is the areal densities for a list of isotopes. These results can be converted to masses by multiplying by the area of the sample in the beam, or mass percentages by simply dividing each by the total areal density. A comparison of the known (ground truth from other NDA) and estimated isotopic weight percentages is given in Table 3. The accuracy is promising given the preliminary nature of these algorithms.

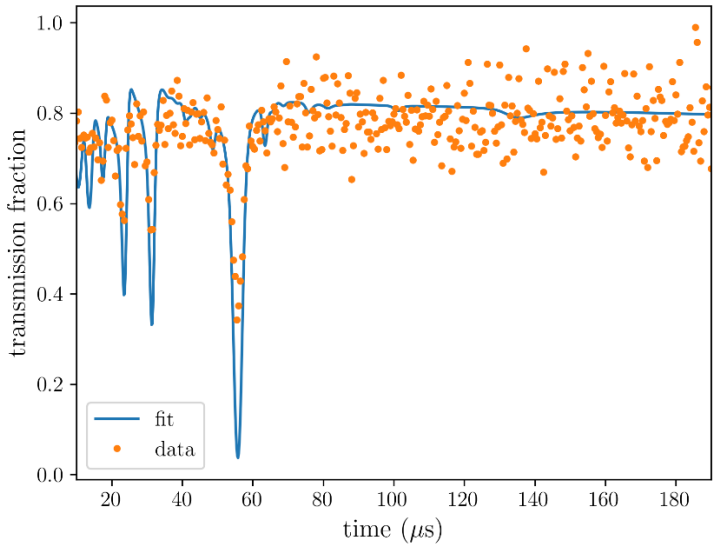

Figure 34. Fit of the NRTA time of flight spectrum (blue) and the measured data (orange) for NRTA data of a depleted uranium plate with 0.3 cm thickness. The plate fully blocks the neutron beam entering the shielded detector.

Table 3. Algorithm results for measured data (depleted uranium plate).

Isotope	Est. g/cm^2	Est. Weight %	NDA weight %
^{234}U	0.004	0.05%	0.007%
^{235}U	0.094	1.13%	0.220%
^{238}U	8.247	98.83%	99.773%

NRTA data with HEU was also acquired and the isotopic composition was estimated. This fit is shown in Figure 35 and summarized in Table 4. The data here look noisier than that with the DU plate. This is reflected in uncertainties in the fitting routine, which are upwards of about 20%. The uncertainty is calculated from the optimization algorithm using derivatives of the optimization problem at the solution. These are numerical uncertainties from the fitting routine only. Nevertheless, given the uncertainties from the algorithm and the ground truth given by NDA, the estimates for ^{234}U and ^{235}U are within their respective errors.

From the estimated areal densities, a total estimated thickness can be calculated, assuming an estimated density of 18.72 g/cm^3. For the HEU sample, this was estimated to be 0.6 mm, though the actual was 1 mm. For the DU sample and assuming an 18.95 g/cm^3 density, the estimated thickness was 4.4 mm, while the actual was 3 mm. Large errors here indicate that updates to the physics model are needed, though the estimated weight percent values for the isotopes are closer to the actuals.

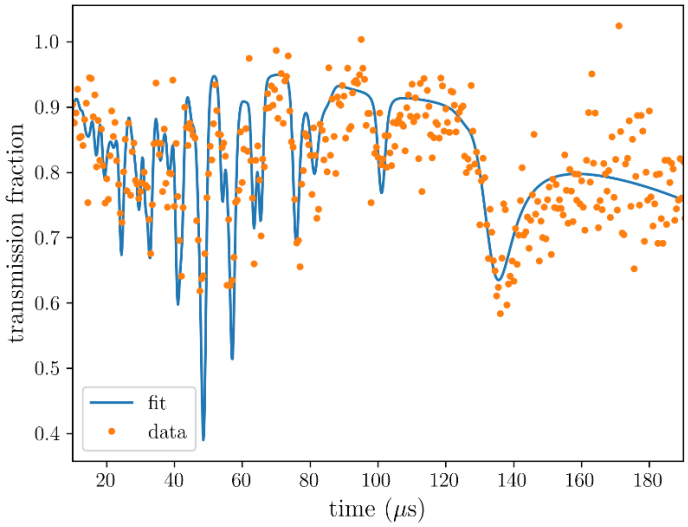

Figure 35. Fit of an NRTA measurement to measured data of an HEU plate.

Table 4. Algorithm results fitting to measured data of an HEU plate.

Isotope	Est. g/cm^2	Est. Weight %	NDA weight %
^{234}U	0.01 ± 0.002	0.8 ± 0.2	0.97 ± 0.12
^{235}U	1.177 ± 0.2	97.1 ± 16.5	91.28 ± 11.18
^{238}U	0.026 ± 0.016	2.1 ± 1.3	7.75 ± 2.44

These initial quantitative isotopic estimation results are encouraging, though more work needs to be done to increase the accuracy of the physics model, such as adding in a realistic background term. Further, regions of fitting could be reduced depending on the isotope to reduce fitting errors. Another piece of software is available which can do similar fitting to NRTA data, the REFIT-2009 package (Moxon et al. 2010). This software uses a much more complex physics model that could potentially outperform the algorithm being developed here. The research team has the software now and will begin testing it this fiscal year and comparing it to the team's fitting algorithm.

This page intentionally left blank.

7.0 Conclusions and Future Work

In the first year of this project, the research team completed a diverse range of tasks to demonstrate the feasibility of NRTA for thorium fuel cycle NDA. The research team characterized ^{233}U material at PNNL, identified other relevant sources for testing, designed and fabricated custom NRTA source holders, explored sample measurement configurations in modeling space, surveyed and down-selected neutron detectors, made initial NRTA measurements with a thorium source, and developed an algorithm that initially works very well on measured data.

Key findings included:

- The ^{233}U material at PNNL is very pure, which will be helpful for testing quantitative NRTA methods.
- Samples with ^{232}Th, ^{235}U, ^{233}U, ^{238}U, and ^{239}Pu are available for measurements and can be stacked to create different isotope areal densities for testing quantitative algorithms.
- Initial analysis on NRTA data of ^{232}Th showed that it was possible to detect resonances of that isotope in a relevant sample configuration.
- An initial analysis algorithm performed surprisingly well for accurately estimating uranium isotopics in measured DU and HEU objects.

In the remaining year of the project, the research team plans to tackle the following tasks:

- Refine the MCNP model to achieve good agreement with measured data, such that it can be used for predictive simulations. Model expected NRTA TOF spectra for estimated MSR salt compositions.
- Prepare and measure samples, including ^{233}U.
- Refine algorithm, assess performance, and compare with REFIT.

This page intentionally left blank.

8.0 References

Behrens, James W., Ronald G. Johnson, and Roald A. Schrack. 1984. "Neutron Resonance Transmission Analysis of Reactor Fuel Samples." *Nuclear Technology* 67 (1): 162-168. https://doi.org/10.13182/NT84-A33538.

Berlizov, Andrey, Andreas Schachinger, Klaus Roetsch, Nicole Erdmann, Helene Schorlé, Martin Vargas, Jozsef Zsigrai, Aleksandr Kulko, Miroslav Keselica, and Fabien Caillou. 2016. "Feedback from Operational Experience of on-Site Deployment of Bias Defect Analysis with COMPUCEA." *Journal of Radioanalytical and Nuclear Chemistry* 307 (3): 1901-1909. https://doi.org/https://doi.org/10.1007/s10967-015-4364-2.

Betzler, Benjamin R., Jeffrey J. Powers, and Andrew Worrall. 2017. "Molten Salt Reactor Neutronics and Fuel Cycle Modeling and Simulation with Scale." *Annals of Nuclear Energy* 101: 489-503. https://doi.org/https://doi.org/10.1016/j.anucene.2016.11.040. https://www.sciencedirect.com/science/article/pii/S0306454916309185.

Burnett, Jonathan L. 2022. "A Safeguards Approach for Molten Salt Reactors: Direct Gamma-Spectrometry of ^{233}U." *Nuclear Instruments and Methods in Physics Research Section A: Accelerators, Spectrometers, Detectors and Associated Equipment* 1031: 166467. https://doi.org/https://doi.org/10.1016/j.nima.2022.166467.

Chichester, David L, and James W Sterbentz. 2012. *Assessing the Feasibility of Using Neutron Resonance Transmission Analysis (NRTA) for Assaying Plutonium in Spent Fuel Assemblies.* Idaho National Laboratory (INL) (Idaho Falls, ID). INL/CON-12-24555. https://inldigitallibrary.inl.gov/sites/sti/sti/5517268.pdf.

Dion, Mike, Louise G Worrall, Stephen Croft, and Logan Scott. 2021. *Molten Salt Reactor Signatures and Modeling Study.* Oak Ridge National Lab.(ORNL), Oak Ridge, TN (United States). ORNL/SPR-2020/1836. https://doi.org/10.2172/1761616.

Engel, Ezra M, and Areg Danagoulian. 2019. "A Physically Cryptographic Warhead Verification System Using Neutron Induced Nuclear Resonances." *Nature communications* 10 (1): 1-10. https://doi.org/https://doi.org/10.1038/s41467-019-12386-0.

Engel, Ezra M, Ethan A Klein, and Areg Danagoulian. 2020. "Feasibility Study of a Compact Neutron Resonance Transmission Analysis Instrument." *AIP Advances* 10 (1): 015051. https://doi.org/https://doi.org/10.1063/1.5129961.

Evans, Louise G, Vlad Henzl, Alicia Swift, Nicholas P Luciano, Eric Cervi, Jill Cooley, Bryn Davies, Joanna S Denton, Andrea Favalli, and Brandon Grogan. 2021. *Safeguards Technology for Thorium Fuel Cycles: Research and Development Needs Assessment and Recommendations.* Oak Ridge National Lab (ORNL) (Oak Ridge, TN). ORNL/TM-2020/1866. https://info.ornl.gov/sites/publications/Files/Pub150423.pdf.

Gilbert, Andrew J., Benjamin S. McDonald, Sean M. Robinson, Ken D. Jarman, Tim A. White, and Mark R. Deinert. 2014. "Non-Invasive Material Discrimination Using Spectral X-Ray Radiography." *Journal of Applied Physics* 115 (15): 154901. https://doi.org/https://doi.org/10.1063/1.4870043.

Hasemi, H, M Harada, T Kai, T Shinohara, M Ooi, H Sato, K Kino, M Segawa, T Kamiyama, and Y Kiyanagi. 2015. "Evaluation of Nuclide Density by Neutron Resonance Transmission at the Noboru Instrument in J-Parc/Mlf." *Nuclear Instruments and Methods in Physics Research Section A: Accelerators, Spectrometers, Detectors and Associated Equipment* 773: 137-149. https://doi.org/https://doi.org/10.1016/j.nima.2014.11.036.

Houtzeel, A., and F. F. Dyer. 1972. *Study of Fission Products in the Molten-Salt Reactor Experiment by Gamma Spectrometry.* Oak Ridge National Laboratory https://www.osti.gov/servlets/purl/4659054.

Klein, Ethan, Farheen Naqvi, Jacob Bickus, Hin Lee, Areg Danagoulian, and Robert Goldston. 2021. "Neutron-Resonance Transmission Analysis with a Compact Deuterium-Tritium Neutron Generator." *Physical Review Applied* 15 (5): 054026. https://doi.org/10.1103/PhysRevApplied.15.054026.

Klein, Ethan, Farheen Naqvi, and Areg Danagoulian. 2021. "Neutron Resonance Transmission Analysis (NRTA) for Nuclear Fuel Characterization Using a Portable Dt Neutron Generator." Annual Meeting of the Institute of Nuclear Materials Management. https://resources.inmm.org/sites/default/files/2021-09/a114.pdf.

Kovacic, Donald N, Andrew Worrall, Louise G Worrall, George F Flanagan, David Eugene Holcomb, Robert Bari, Lap Cheng, David Farley, and Matthew Sternat. 2018. "Safeguards Challenges for Molten Salt Reactors." INMM Annual Meeting, Baltimore, MD. https://www.osti.gov/servlets/purl/1474868.

Losko, Adrian S, Sven C Vogel, Mark A Bourke, Stewart L Voit, Ken J McClellan, Michael Mocko, Darrin D Byler, Anton S Tremsin, and Peter Hosemann. 2016. "Characterization of Fresh Nuclear Fuel Using Time-of-Flight Neutrons." *Transactions of the American Nuclear Society* 114 (1). https://atlas-scientific.com/product/ezo-humidity-circuit/.

Losko, Adrian Simon, and SC Vogel. 2022. "3D Isotope Density Measurements by Energy-Resolved Neutron Imaging." *Scientific Reports* 12 (1): 1-7. https://doi.org/https://doi.org/10.1038/s41598-022-10085-3.

Losko, AS, Y Han, B Schillinger, A Tartaglione, M Morgano, M Strobl, J Long, AS Tremsin, and M Schulz. 2021. "New Perspectives for Neutron Imaging through Advanced Event-Mode Data Acquisition." *Scientific Reports* 11 (1): 1-11. https://doi.org/https://doi.org/10.1038/s41598-021-00822-5.

Marshall, Matthew SJ, Mitali J More, Harish B Bhandari, Richard A Riedel, Shane Waterman, John Crespi, Peter Nickerson, Stuart Miller, and Vivek V Nagarkar. 2017. "Novel Neutron Detector Material: Microcolumnar Li X Na 1–X I: Eu." *IEEE Transactions on Nuclear Science* 64 (11): 2878-2882. https://doi.org/10.1109/TNS.2017.2762859.

McDonald, B.S., J.L. Burnett, R.A. Clark, A. Danagoulian, A.J. Gilbert, M.E. Moore, J.A. Kulisek, E.A. Klein, G.A. Warren, and M.A. Zalavadia. 2022. "New NDA Methods for Thorium Fuel Cycle Safeguards " Annual Meeting of the Institute of Nuclear Materials Management.

"MCP Neutron Detector." ProxiVision GmbH. https://www.proxivision.de/wp-content/uploads/PV_Neutron-Detector_201611.pdf.

Refit-2009 a Least-Square Fitting Program for Resonance Analysis of Neutron Transmission, Capture, Fission and Scattering Data Users' Guide for Refit-2009-10. UKNSF.

Nagarkar, VV, EE Ovechkina, HB Bhandari, L Soundara-Pandian, MJ More, RA Riedel, and SR Miller. 2015. "New Structured Scintillators for Neutron Radiography." *Physics Procedia* 69: 161-168. https://doi.org/10.1016/j.phpro.2015.07.023.

Postma, H, and P Schillebeeckx. 2017. "Neutron Resonance Analysis." In *Neutron Methods for Archaeology and Cultural Heritage*, edited by N. Kardjilov and G. Festa, 235-283. Swizerland: Springer International Publishing.

Reed, Richard, Louise G Worrall, and Donald N Kovacic. 2022. *Safeguards for the Lithium Fluoride Thorium Reactor: A Preliminary Nuclear Material Control and Accounting Assessment.* Oak Ridge National Lab.(ORNL), Oak Ridge, TN (United States). ORNL/TM-2022/2394. https://www.osti.gov/servlets/purl/1881125/.

Sagadevan, Athena, Daniela Henzlova, Howard Menlove, Mark Croce, Michael Dion, Robert Morris, and Bruce Bevard. 2021. *Experimental Validation of NDA for Msr Safeguards Fy21 Report.* LA-UR-21-29908, ORNL/TM-2021/2288. https://gain.inl.gov/SiteAssets/AdvancedReactorSafeguards/KeyThrustArea4/M3RS-21LA0401051_NDA_for_MSRs_FY21_Report_%20FINAL.pdf.

Schwarz, A.L., R.A. Schwarz, and A.R. Schwarz. 2018. *MCNPX/6 Visual Editor Computer Code Manual.*

Sterbentz, James W, and David L Chichester. 2011. *A Second Look at Neutron Resonance Transmission Analysis as a Spent Fuel NDA Technique.* Idaho National Laboratory (INL). INL/CON-11-20783

TRN: US1103285. https://www.osti.gov/biblio/1017872.

Swift, Alicia, Karen Hogue, Thomas Folk, and Jill Cooley. 2020. *Safeguards Technical Objectives for Thorium Molten Salt Reactor Fuel Cycles.* Oak Ridge Y-12 Plant (Y-12), Oak Ridge, TN (United States) https://www.osti.gov/servlets/purl/1763719.

Tan, Jinhao, Yushou Song, Jianrong Zhou, Jianjin Zhou, Xingfen Jiang, Xiaojuan Zhou, Wenqin Yang, Yuanguang Xia, Shulin Liu, and Baojun Yan. 2022. "Novel Method to Improve Neutron–Gamma Discrimination for Boron-Doped Nmcps." *Nuclear Instruments and Methods in Physics Research Section A: Accelerators, Spectrometers, Detectors and Associated Equipment*: 167828. https://doi.org/https://doi.org/10.1016/j.nima.2022.167828.

Tremsin, AS, AE Craft, MAM Bourke, AT Smolinski, GC Papaioannou, MA Ruddell, J Littell, and J Tedesco. 2018. "Digital Neutron and Gamma-Ray Radiography in High Radiation Environments with an MCP/Timepix Detector." *Nuclear Instruments and Methods in Physics Research Section A: Accelerators, Spectrometers, Detectors and Associated Equipment* 902: 110-116. https://doi.org/https://doi.org/10.1016/j.nima.2018.05.069.

Tsuchiya, H, M Koizumi, F Kitatani, and H Harada. 2019. "Performance of Large Volume $LaBr_3$ Scintillation Detector Equipped with Specially-Designed Shield for Neutron Resonance Capture Analysis." *Nuclear Instruments and Methods in Physics Research Section A: Accelerators, Spectrometers, Detectors and Associated Equipment* 932: 16-26. https://doi.org/https://doi.org/10.1016/j.nima.2019.04.048.

Virtanen, Pauli, Ralf Gommers, Travis E Oliphant, Matt Haberland, Tyler Reddy, David Cournapeau, Evgeni Burovski, Pearu Peterson, Warren Weckesser, and Jonathan Bright. 2020. "Scipy 1.0: Fundamental Algorithms for Scientific Computing in Python." *Nature methods* 17 (3): 261-272. https://doi.org/https://doi.org/10.1038/s41592-019-0686-2.

Wang, Cai-Lin, and Richard A Riedel. 2016. "Improved Neutron-Gamma Discrimination for a 6li-Glass Neutron Detector Using Digital Signal Analysis Methods." *Review of Scientific Instruments* 87 (1): 013301. https://doi.org/10.1063/1.4939821.

Werner, Christopher John, Jeffrey S Bull, Clell Jeffrey Solomon, Forrest B Brown, Gregg Walter McKinney, Michael Evan Rising, David A Dixon, Roger Lee Martz, Henry G Hughes, and Lawrence James Cox. 2018. *MCNP Version 6.2 Release Notes.* Los Alamos National Lab.(LANL), Los Alamos, NM (United States). LA-UR-18-20808. https://mcnp.lanl.gov/pdf_files/la-ur-18-20808.pdf.

Worrall, Louise G, Andrew Worrall, George F Flanagan, Stephen Croft, Alan M Krichinsky, Chris A Pickett, Robert D McElroy Jr, Steven L Cleveland, Donald N Kovacic, and J Michael Whitaker. 2016. "Safeguards Considerations for Thorium Fuel Cycles." *Nuclear Technology* 194 (2): 281-293. https://doi.org/https://doi.org/10.13182/NT15-103.

Zalavadia, M. A., A. Danagoulian, E. A. Kelin, M. E. Moore, F. Naqvi, G. A. Warren, and R. S. Wittman. 2021. *Isotope Verification for Arms Control: Fy21 Progress Report.* Pacific Northwest National Laboratory (Richland, WA). PNNL-31891.

Zhang, Yuxuan, Jean-C Bilheux, Hassina Z Bilheux, and Jiao YY Lin. 2019. "An Interactive Web-Based Tool to Guide the Preparation of Neutron Imaging Experiments at Oak Ridge National Laboratory." *Journal of Physics Communications* 3 (10): 103003. https://doi.org/10.1088/2399-6528/ab4ee6. https://neuit.ornl.gov/resonance.

Pacific Northwest National Laboratory

902 Battelle Boulevard
P.O. Box 999
Richland, WA 99354

1-888-375-PNNL (7665)

www.pnnl.gov